Electronic Theses and Dissertations   Graduate School

2019

Electrochemical Studies Involving CO2 Reduction with Rhenium-based Catalysts and for Guanosine Monophosphate Oxidation

Kayla A. Milano
University of Mississippi

ELECTROCHEMICAL STUDIES INVOLVING CO_2 REDUCTION WITH RHENIUM-

BASED CATALYSTS AND FOR GUANOSINE MONOPHOSPHATE OXIDATION

A Thesis Presented in partial fulfillment of requirements

For the degree of Master of Science

The University of Mississippi

by

KAYLA ANNE MILANO

May 2019

ABSTRACT

The first chapter will cover the reduction of CO_2 with rhenium catalysts. Due to increasing levels of atmospheric greenhouse gases produced from fossil fuel combustion, developing alternative energy sources that are both clean and renewable remains an important research objective. One option being explored is the ability to convert carbon dioxide back into energy-rich fuels. The main problem encountered with the reduction of this greenhouse gas is the negative voltages that are often necessary for conversion to occur. The hypothesis was that by studying known rhenium complexes with additional redox-active ligand substituents that we would be able to build a better fundamental knowledge on the benefits of accessing reducing equivalents for the system and their participation in multi-electron catalysis.

The following chapter will cover the oxidation of guanine monophosphate (GMP). GMP has been linked to numerous disease states when it is oxidized or damaged. There have been two oxidation pathways suggested in association with the oxidation of GMP: EPT and MS-EPT. Concerted electron-proton transfer (concerted EPT) is a donor transferring electron or protons from their orbitals to the orbitals of an acceptor. Multisite electron-proton transfer (MS-EPT) is concerted EPT for multiple donors to a single acceptor or vice versa. The conditions and mechanistic implications for GMP's oxidation has been studied. Our study focused on acetate versus phosphate buffer, varying base concentration in phosphate buffer, and varying the concentration of a ruthenium-based redox mediator.

DEDICATION

My thesis is dedicated to my family and all those who have helped and supported me through this process. They have supported me with any issue that resulted from my Auditory Processing Disorder and other health concerns. They have provided me with advice to handle ever issue that has happened throughout my life and time here.

LIST OF ABBREVIATIONS AND SYMBOLS

Keywords:	Abbreviations:
Guanine monophosphate	GMP
Concerted electron-proton transfer	Concerted EPT
Electron-proton transfer	EPT
Multi-site electron-proton transfer	MS-EPT
H-atom transfer	HAT
Proton transfer-electron transfer	PT-ET
Electron transfer-proton transfer	ET-PT
Tyrosine	Tyr
Tin-doped indium oxide	ITO
Silver-silver chloride	Ag/AgCl
Cyclic voltammetry	CV
Ferrocene	Fc
Micromolar	μM
Carbon Dioxide	CO_2

ACKNOWLEDGEMENTS

TABLE OF CONTENTS

INTRODUCTION

Hydrocarbon fuel accounts for up to 86% of global energy consumption; however, fossil fuels are finite and nonrenewable resources.[1,2] Their ongoing depletion increases the need for more efficient and sustainable energy storage and production.[1] The advancement of undeveloped societies is also strongly correlated with increased consumption of energy.[3] Fossil fuels generate carbon dioxide when used.[2] The emitted carbon dioxide accumulates and concentrates in the atmosphere which causes climate changes to occur.[2]

Due to the increased emission of carbon dioxide since the Industrial Revolution, scientists have focused on understanding the impact of this greenhouse gas in the atmosphere and on developing new technologies to mitigate CO_2 emissions and replace fossil fuels with renewable and carbon neutral energy alternatives. The maximum concentration limit of atmospheric carbon dioxide to avoid catastrophic climate change is anticipated to be 450-500 parts per billion. At the current fossil fuel consumption rate, it is predicted that this critical limit will be met in the next 50 years if no change occurs.[13-16]

A promising strategy to access renewable fuels is to convert carbon dioxide back into a reduced carbon product that can be burned in the usual fashion (combustion engines, gas furnaces, etc). Carbon dioxide, however, is a difficult molecule to activate and reduce as it is nonpolar overall and thermodynamically stable. Catalysts are needed to mediate the reaction and provide lower energy pathways for its conversion into fuels such as methanol or methane, or fuel precursors that can be converted into conventional fuels via Fischer-Tropsch chemistry. In this way, a closed carbon cycle can be achieved as renewable fuels, compatible with existing infrastructure, are

generated from carbon dioxide using catalysts, which results in zero net gain in atmospheric CO_2. Existing catalysts often have high overpotentials, low stability, and poor selectivity. Thus, the development of better catalysts is a critical area of research to enable new technologies for alternative fuels. In these technologies, renewable electricity or sunlight provides the energy necessary to drive the catalytic conversion of CO_2 into desired fuels and commodity products. Herein, we have targeted rhenium-based electrocatalysts that can be driven electrochemically to mediate CO_2 reduction to carbon monoxide (CO).

2,2':6',2"- terpyridine (tpy) is a heterocyclic nitrogen-donor ligand. Terpyridine can bind to metals as a tridentate ligand with meridianol (mer) coordination. If the ligand is unable to bind in a meridianol fashion, then the ligand can bind to the metal as a bidentate ligand where one of the pyridyl donors remains uncoordinated.[5] Terpyridine's ability to act as a bidentate ligand has been seen in thermal reaction pathways and products of photolysis of tridentate tpy complexes. Rhenium (Re) is a low-spin, third-row transition metal. The compound $Re(tpy)(CO)_3Cl$ has been structurally characterized and contains a facial arrangement of the three carbonyl donors and a bidentate tpy ligand. The uncoordinated pyridyl ring is not coplanar with the other two rings due to a steric interaction with a carbonyl group.[5]

In electrochemical processes, the electrolyte solution allows for current to pass efficiently by aiding in the movement of electrons from the anode to the cathode.[4] Reduction of the electroactive species occurs by electron transfer from the cathode to the species in solution. An associated oxidation must also occur involving the same overall number of electrons at the counter electrode (anode in this case), which could be solvent or electrolyte decomposition.[4]

Polypyridines have proven to be vital in creating successful redox complexes employing numerous metals for carbon dioxide reduction. In general, such complexes have been applied to

photoactivated electron transfer reactions and applications for energy conversions.[6,7] Polypyridyl complexes often have well-defined ligand-based reductions that can be accessed at modest potentials. The multielectron reduction of electrocatalysts is advantageous for facilitating the multielectron conversion of CO_2. In addition, these metal complexes are tunable based on which metal is used and by ligand design where the chemistry and redox potentials of the catalyst can be altered by rational and systematic ligand modifications.[5,7]

Metalating tpy with rhenium allows for a robust bonding interaction given the bidentate coordination of the ligand while leaving a pendant pyridine group in close proximity to the active site. The complex can be tuned by methylation of the pendant pyridine to form a methylpyridinium moiety. The reduction potentials of the parent tpy complex and its methylated counterpart should be significantly different. The methylated complex is expected to have lower reduction potentials relative to its unmethylated analogue due to the positive charge as well as an additional reduction due to the easily reduced methylpyridinium moiety.

EXPERIMENTAL DETAILS

Electrochemical studies were conducted in a standard three-electrode cell using a glassy carbon disk (3 mm diameter) working electrode, a silver wire quasi-reference electrode, and a platinum wire counter electrode. The potential was referenced at the end of experiments by adding ferrocene as an internal standard.

COMPUTATIONAL DETAILS

William Earwood provided computational results with the following calculation details. Self-consistent field calculations were performed within the Kohn-Sham DFT framework, using a

spin-unrestricted molecular orbital basis. The long-range corrected, hybrid exchange-correlation functional with empirical dispersion corrections, wB97XD, was used for optimizations and single-point energies. Due to the presence of rhenium, the LanL2DZ basis set was used, which uses D95V for first-row species and the Los Alamos ECP plus DZ basis for all other elements, in this case Cl and Re. Analytic gradients converged the maximum and RMS forces (Hartrees/Bohr) to within 1.5E-5 and 1.0E-5, respectively, while maximum and RMS displacements (Angstroms) were limited to 6.0E-5 and 4.0E-5, respectively. An integration grid of 75 radial shells and 302 angular points was used. RMS and maximum density matrix convergence tolerances were 1.0E-8 and 1.0E-6, respectively. All calculations were performed within Gaussian 09, along with a Natural Population Analysis (NPA). Multiwfn was used to localize the occupied canonical orbitals using the Foster-Boys scheme, with a convergence of 1.0E-4. Charge Model 5 (CM5), Mulliken, and Lowdin charges were computed using the same software. Orbital visualization was carried out in Avogadro.
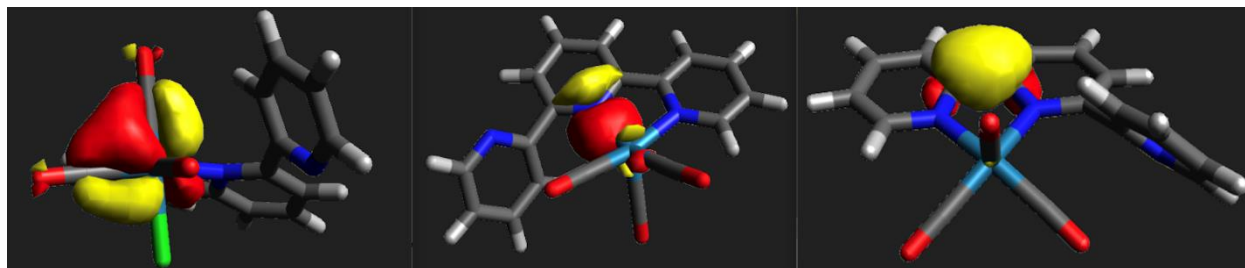
Figure 1. The depiction on the left shows the optimized structure of the neutral unmethylated rhenium κ^2-terpyridine complex, $Re(\kappa^2\text{-tpy})(CO)_3Cl$. Each depiction going to the right is reduced by one-electron and corresponds to the resulting intermediates after dissociation of the chloride ligand. The highest occupied molecular orbital (HOMO) of each optimized structure is also shown.
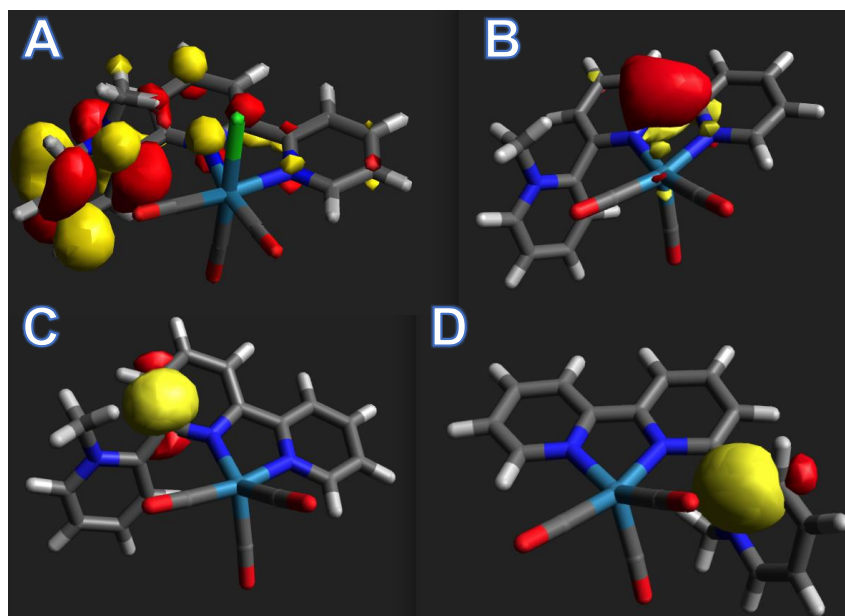
Figure 2. Depiction (A) is the optimized structure of the methylated κ^2-terpyridine rhenium complex. Depictions (B), (C), and (D) are reduced by one-, two-, and three-electrons, respectively, and correspond to the resulting intermediates after dissociation of the chloride ligand. The HOMO of each optimized structure is also shown.

The figures above are the computational structures of the unmethylated (**Figure 1**) and methylated (**Figure 2**) rhenium complexes. As the compound is reduced, the chloride dissociates to open a coordination site for CO_2 activation. The initial compound and reduced five-coordinate intermediates were computed for each complex, as shown in **Figures 1** and **2**, in order to rationalize reactivity and predict where the added electrons reside in the compounds. The highest occupied molecular orbital (HOMO) is shown for each species. In **Figure 1**, the electron density following the first reduction is localized near the rhenium center and the central pyridine ring of the

terpyridine. With the second reduction, the electron density becomes localized on the polypyridyl ligand between the two pyridines that are coordinated to rhenium. In the series of diagrams in **Figure 2**, the electron density of the HOMO is localized primarily on the methylpyridine moiety. After the first reduction, the HOMO is localized on the tpy ligand close to the metal center, but with additional reductions, it moves across the polypyridyl framework and onto the methylated nitrogen. The electron density change from the coordinated bipyridine fragment to the methylated pyridine is rationalized by the need to compensate for the positive charge on the pendant group.

RESULTS

The redox properties of the two compounds were investigated electrochemically using cyclic voltammetry. The cyclic voltammetry was conducted in *N,N*-dimethylformamide (DMF) with a glassy carbon disk working electrode. Results are shown in which each reduction is isolated before the potential is scanned more negatively to include subsequent reductions. Studies were conducted under both nitrogen (N_2) and carbon dioxide atmospheres in order to see the electrocatalytic activity of the compound in the absence and presence of the substrate (CO_2).
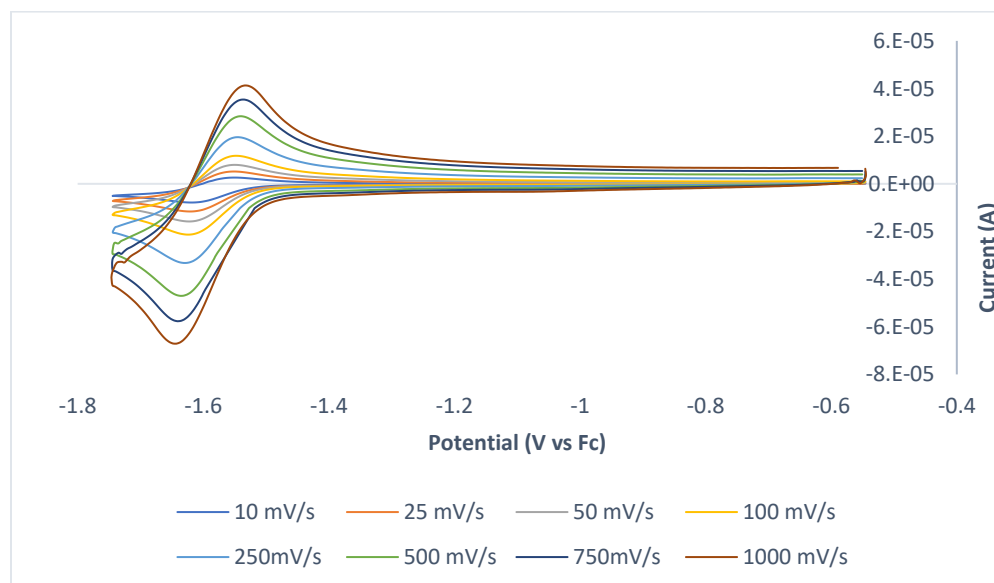
Figure 3. First wave cyclic voltammogram of 2 mM Re(tpy)(CO)$_3$Cl under nitrogen atmosphere in 0.2 M NBu$_4$PF$_6$ in DMF.
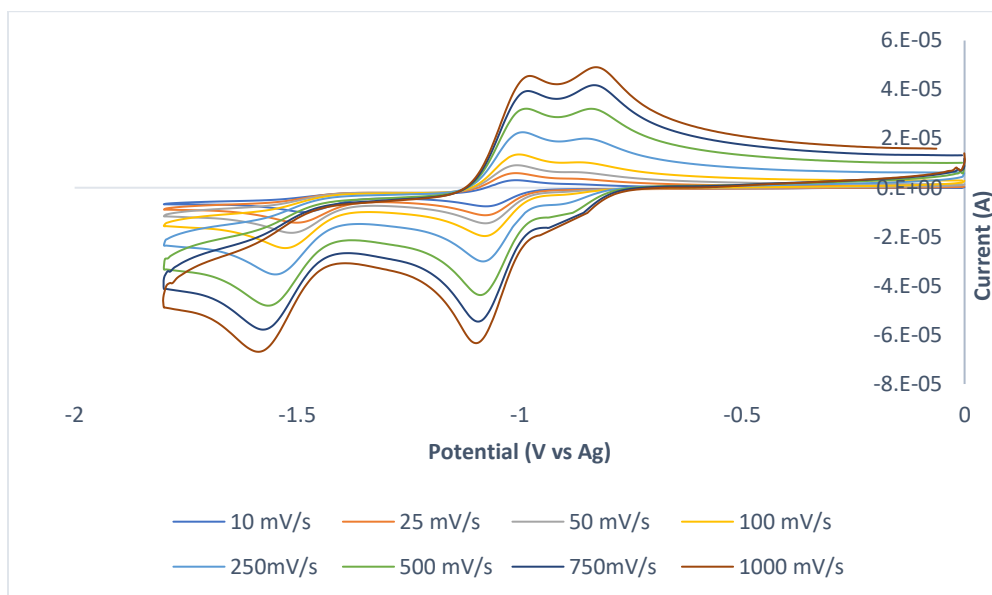
Figure 4. Second wave cyclic voltammograms of 2 mM Re(tpy)(CO)$_3$Cl under nitrogen atmosphere in 0.2 M NBu$_4$PF$_6$ in DMF.
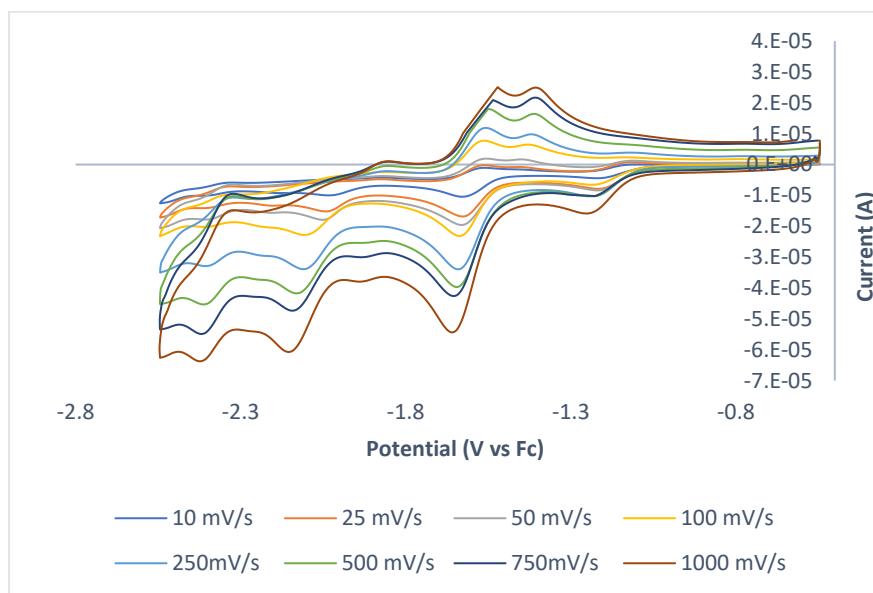
Figure 5. Cyclic voltammograms of 2 mM Re(tpy)(CO)$_3$Cl under nitrogen atmosphere in 0.2 M NBu$_4$PF$_6$ in DMF.
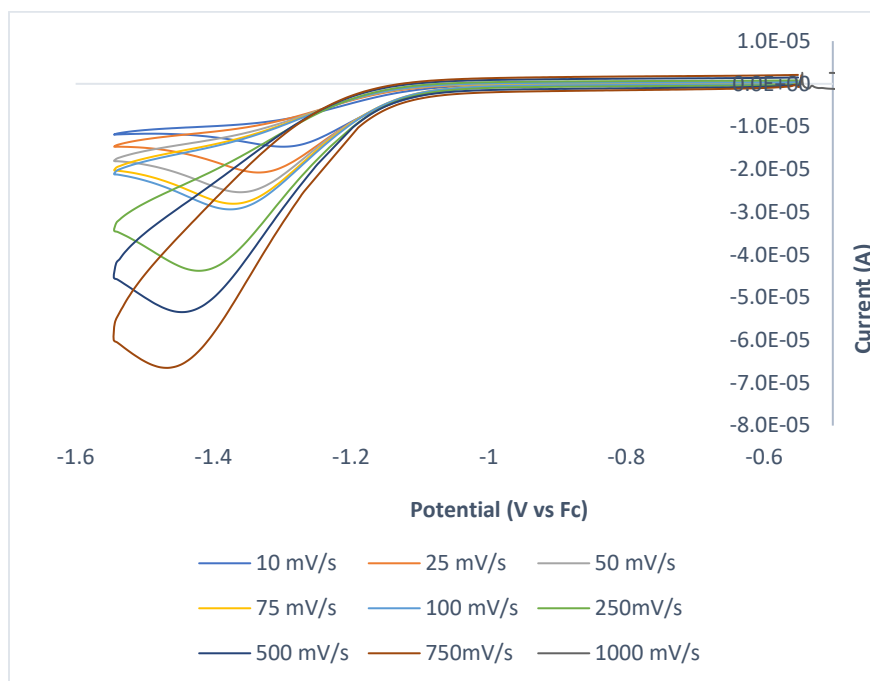
Figure 6. First wave cyclic voltammograms of 2 mM Re(tpy)(CO)$_3$Cl under carbon dioxide atmosphere in 0.2 M NBu$_4$PF$_6$ in DMF.
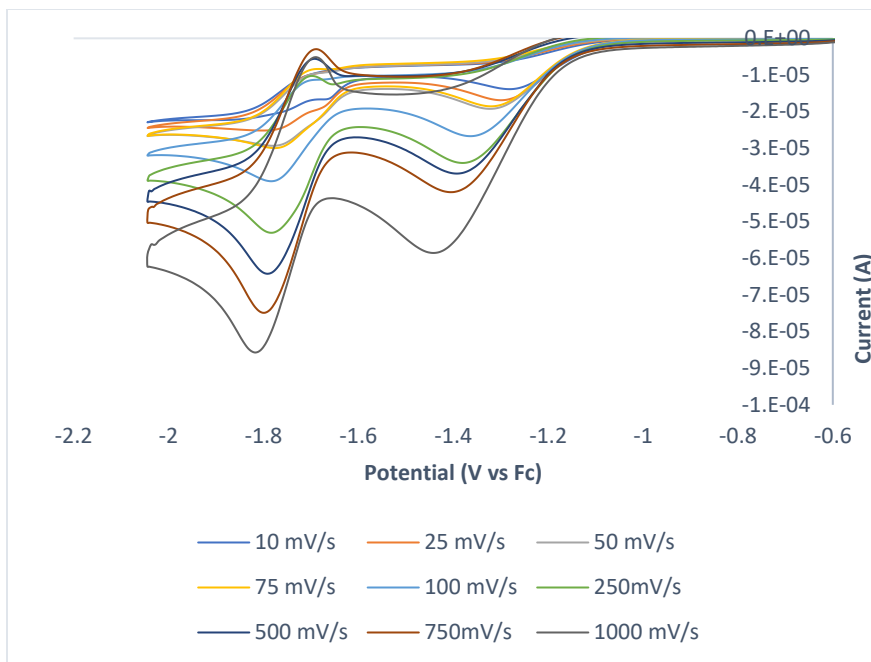
Figure 7. Second wave cyclic voltammograms of 2 mM Re(tpy)(CO)$_3$Cl under carbon dioxide atmosphere in 0.2 M NBu$_4$PF$_6$ in DMF.
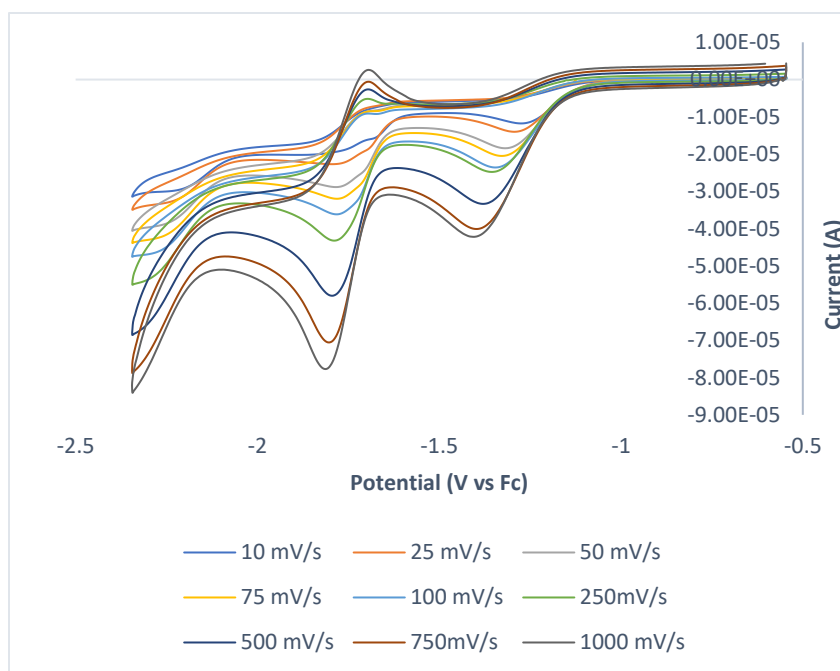
Figure 8. Third wave cyclic voltammograms of 2 mM Re(tpy)(CO)$_3$Cl under carbon dioxide atmosphere in 0.2 M NBu$_4$PF$_6$ in DMF.
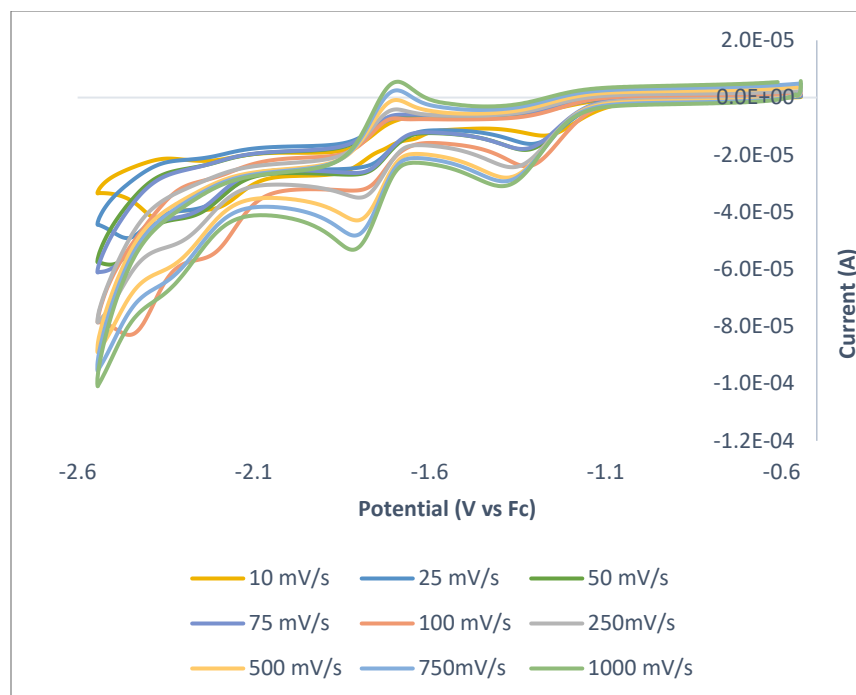
Figure 9. Cyclic voltammograms of 2 mM Re(tpy)(CO)$_3$Cl under carbon dioxide atmosphere in 0.2 M NBu$_4$PF$_6$ in DMF.
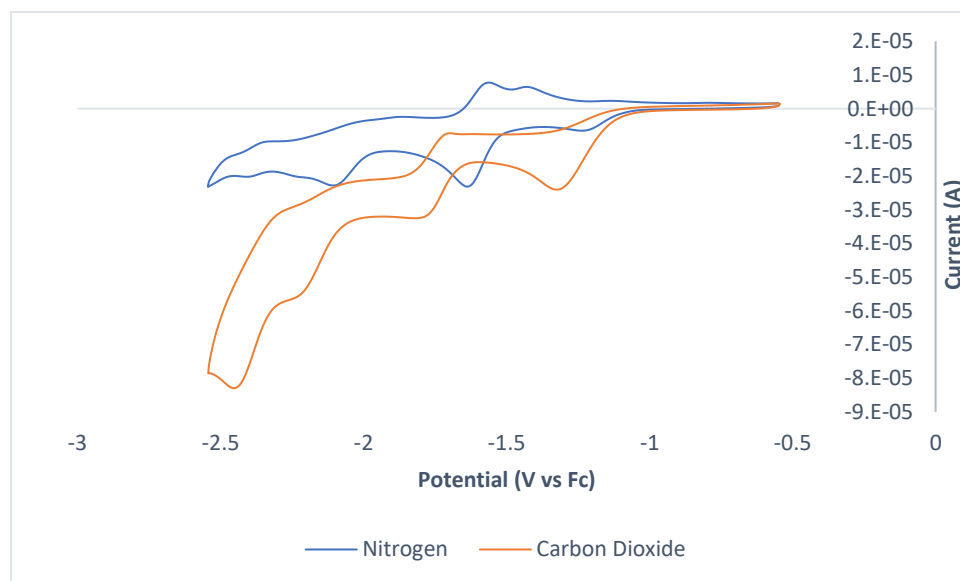
Figure 10. Cyclic voltammograms of 2 mM Re(tpy)(CO)$_3$Cl under listed atmosphere in 0.2 M NBu$_4$PF$_6$ in DMF.
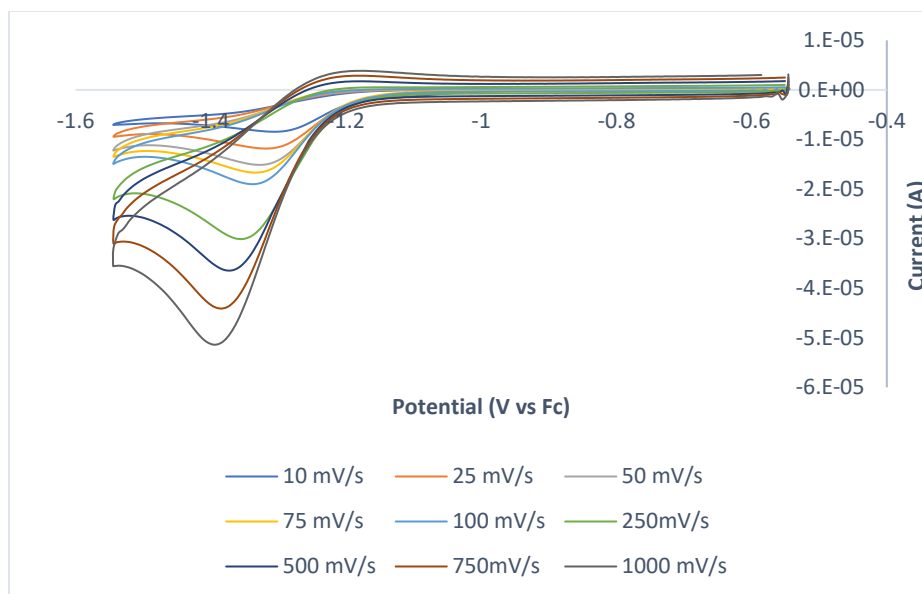
Figure 11. First wave cyclic voltammograms of 2 mM methylated Re(tpy)(CO)$_3$Cl under nitrogen atmosphere in 0.2 M NBu$_4$PF$_6$ in DMF.
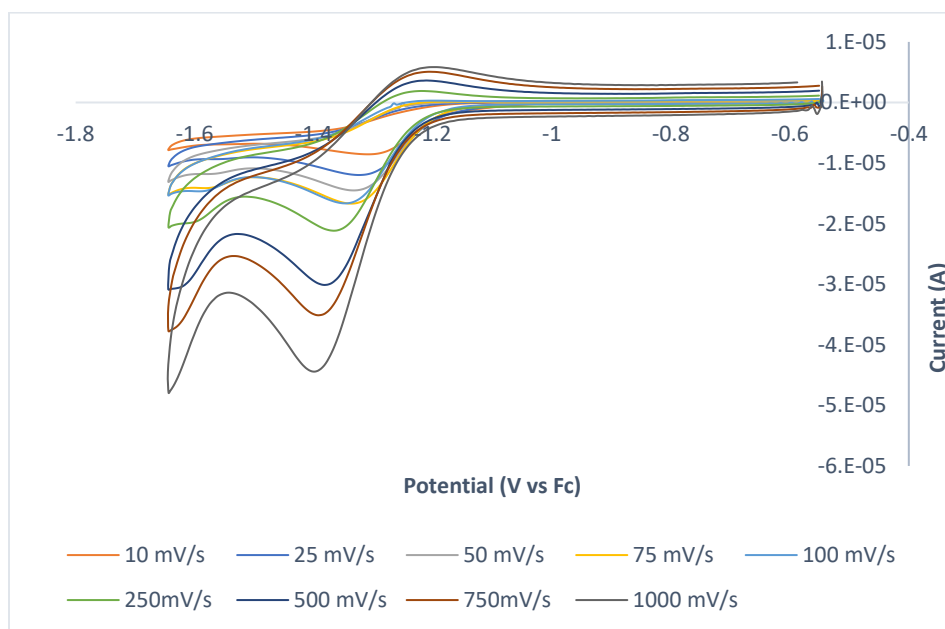
Figure 12. Second wave cyclic voltammograms of 2 mM methylated Re(tpy)(CO)$_3$Cl under nitrogen atmosphere in 0.2 M NBu$_4$PF$_6$ in DMF.
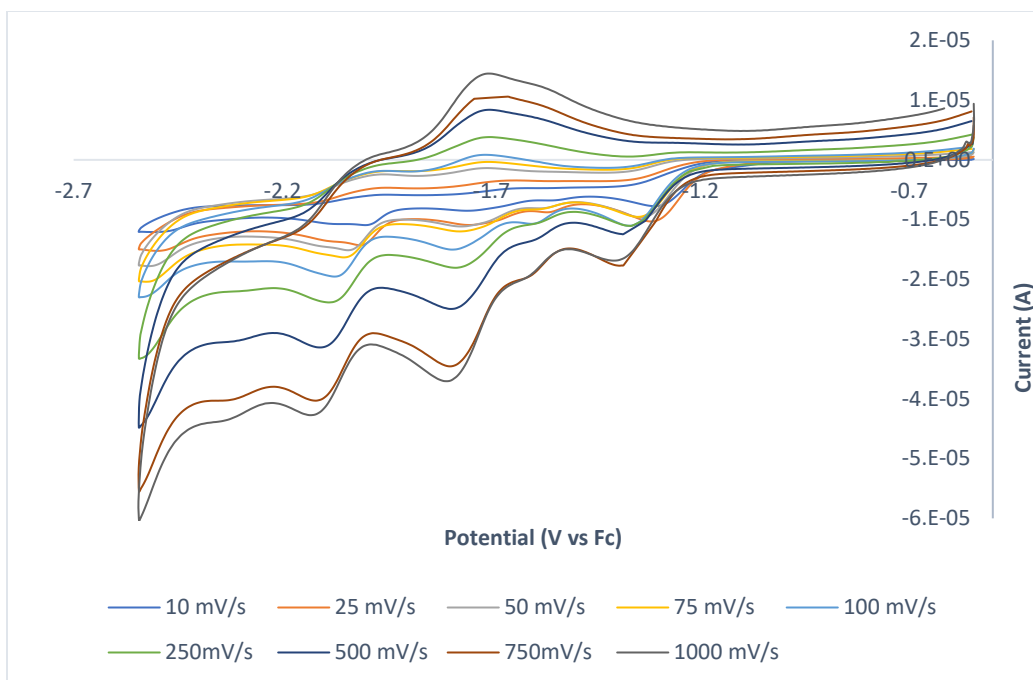
Figure 13. Cyclic voltammograms of 2 mM methylated Re(tpy)(CO)$_3$Cl under nitrogen atmosphere in 0.2 M NBu$_4$PF$_6$ in DMF.
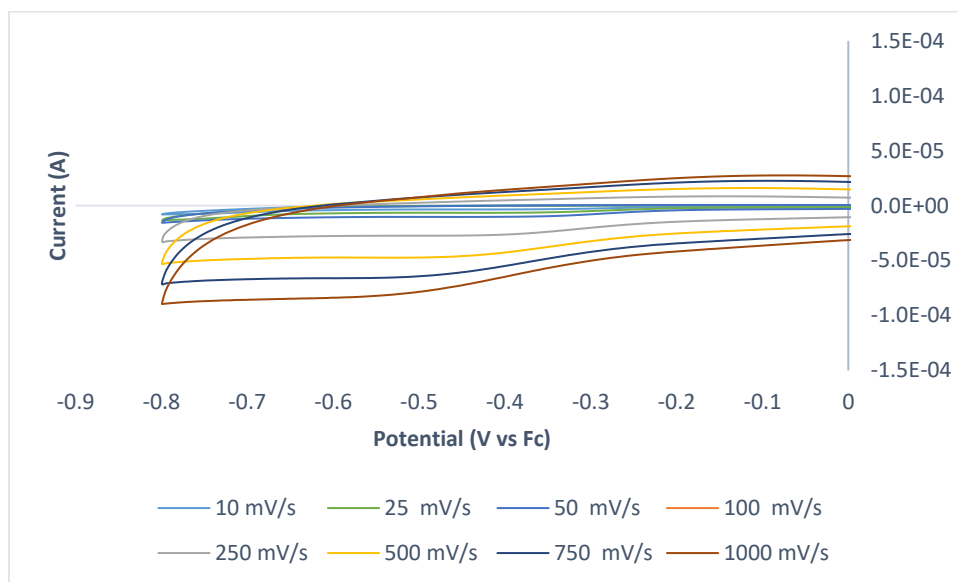
Figure 14. First wave cyclic voltammogram of 2 mM methylated Re(tpy)(CO)$_3$Cl under carbon dioxide atmosphere in 0.2 M NBu$_4$PF$_6$ in DMF.
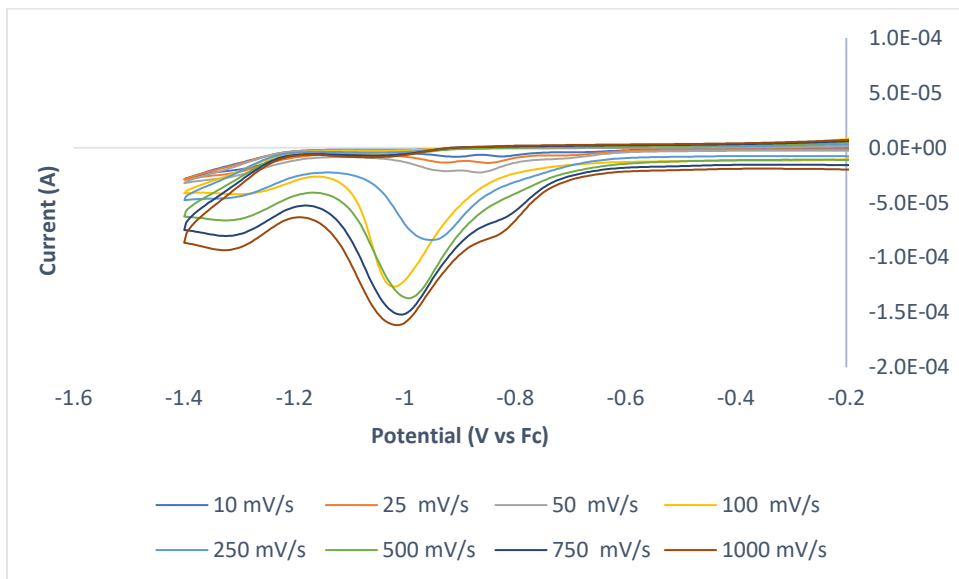
Figure 15. Second wave cyclic voltammograms of 2 mM methylated Re(tpy)(CO)$_3$Cl under carbon dioxide atmosphere in 0.2 M NBu$_4$PF$_6$ in DMF.
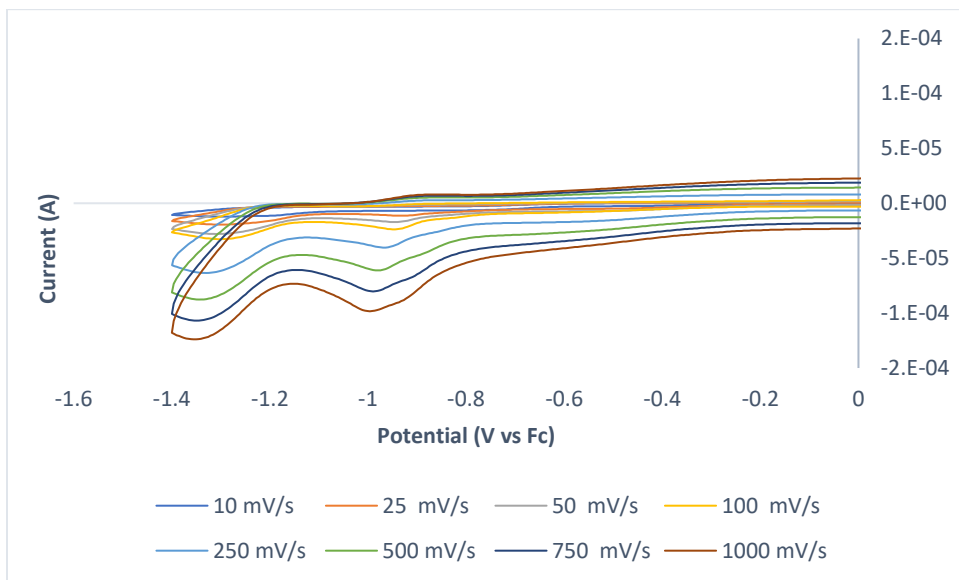
Figure 16. Cyclic voltammograms of 2 mM methylated Re(tpy)(CO)$_3$Cl under carbon dioxide atmosphere in 0.2 M NBu$_4$PF$_6$ in DMF.
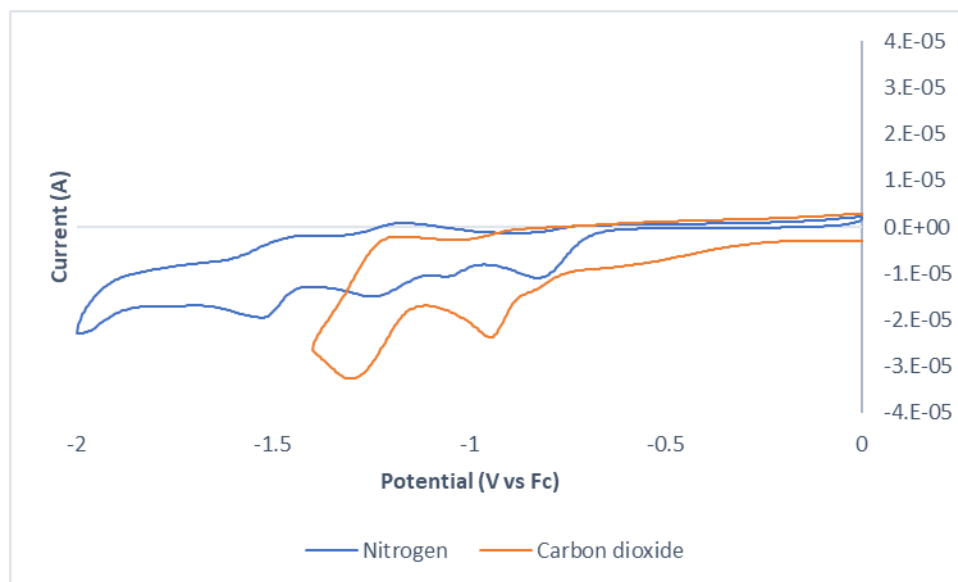
Figure 17. Cyclic voltammograms of 2 mM methylated Re(tpy)(CO)$_3$Cl under listed atmosphere in 0.2 M NBu$_4$PF$_6$ in DMF.
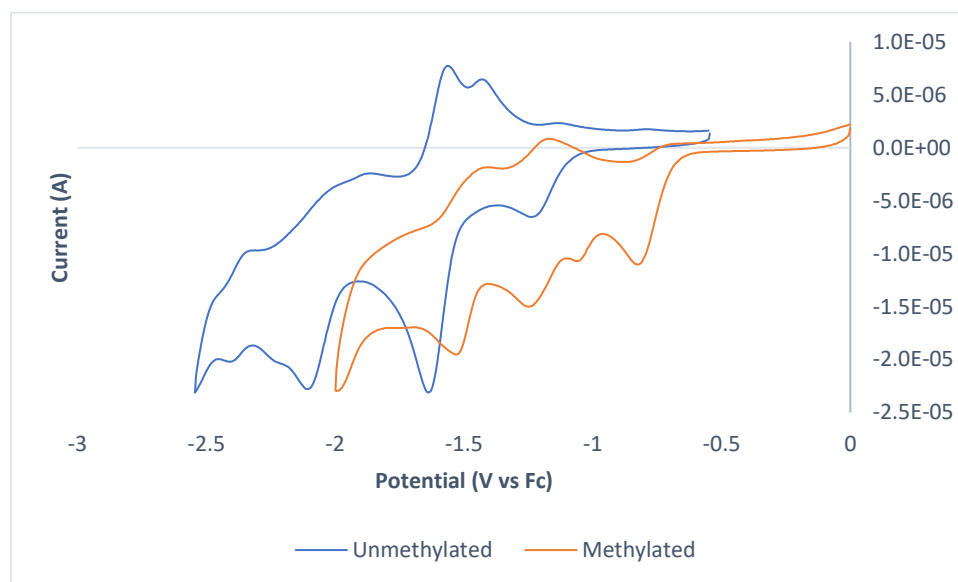
Figure 18. Cyclic voltammograms of 2 mM Re-complex listed under nitrogen atmosphere in 0.2 M NBu$_4$PF$_6$ in DMF.
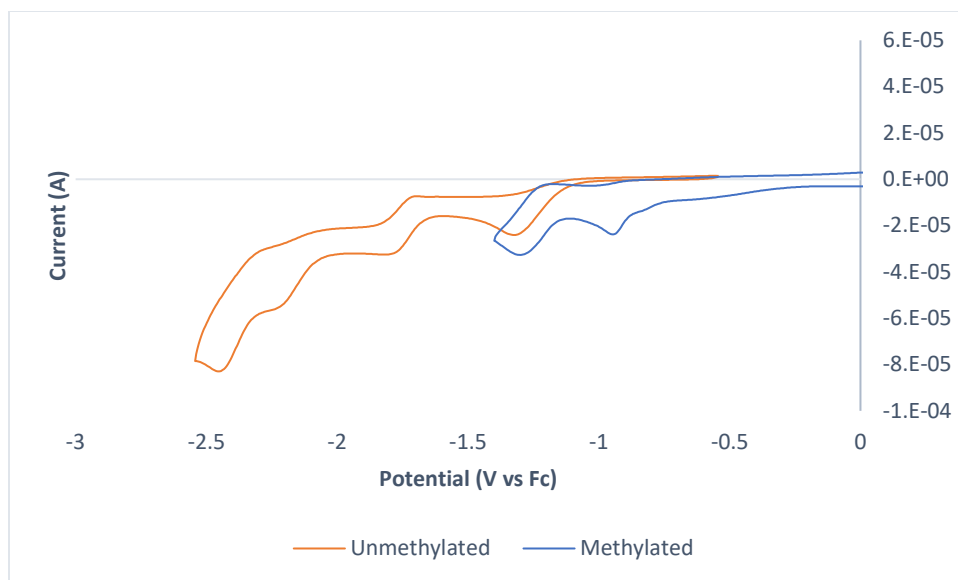
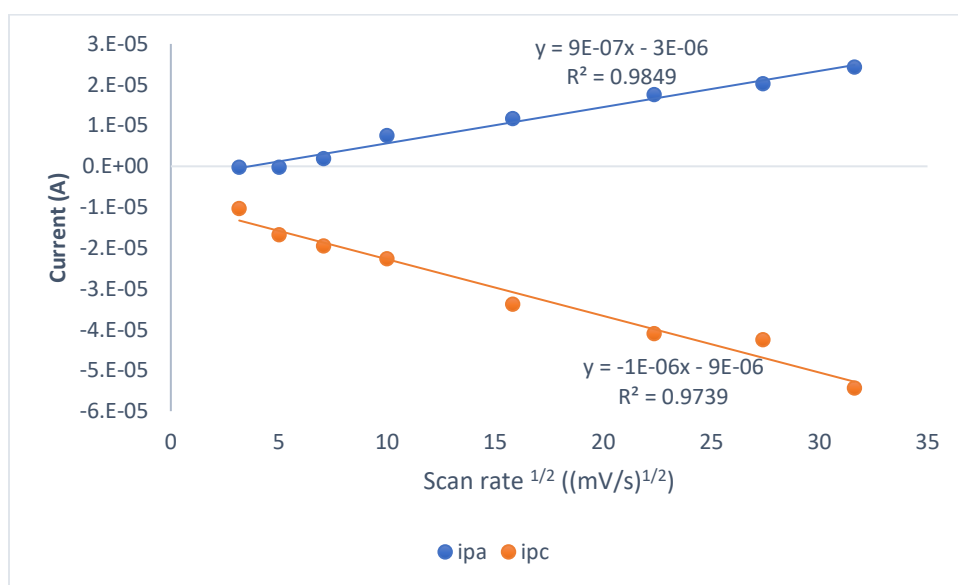**Figure 19.** Cyclic voltammograms of 2 mM Re-complex listed under carbon dioxide atmosphere in 0.2 M NBu_4PF_6 in DMF.

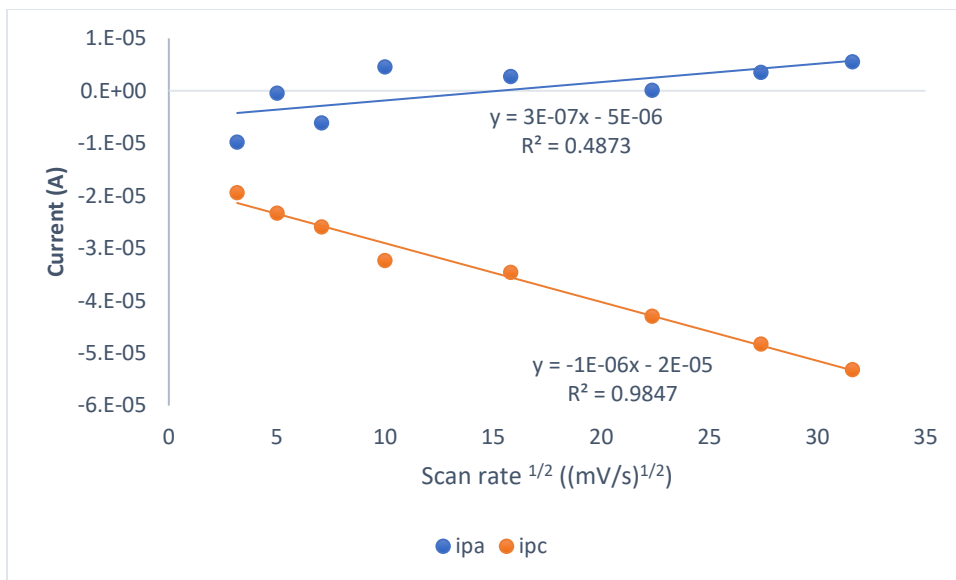**Figure 20.** Scan rate dependence of $Re(tpy)(CO)_3Cl$ under nitrogen atmosphere.

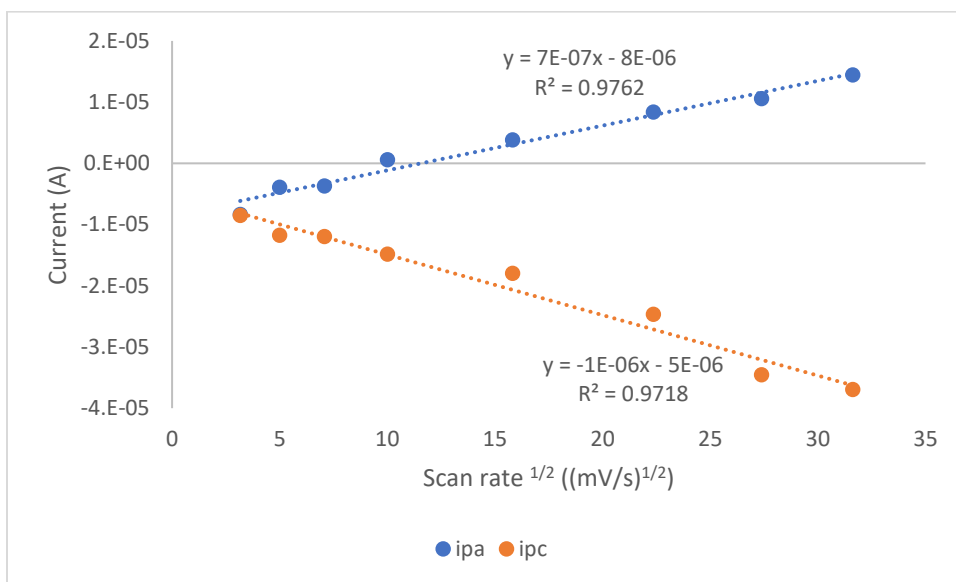**Figure 21.** Scan rate dependence of Re(tpy)(CO)$_3$Cl under carbon dioxide atmosphere.

Figure 22. Scan rate dependence of methylated Re(tpy)(CO)$_3$Cl under nitrogen atmosphere.

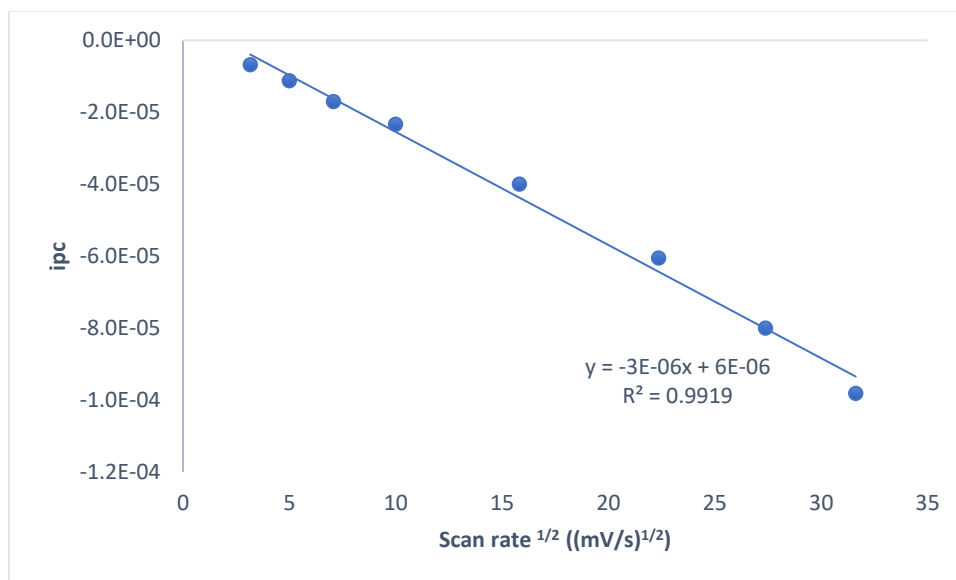**Figure 23.** Scan rate dependence of methylated Re(tpy)(CO)$_3$Cl under carbon dioxide atmosphere.

DISCUSSION

Despite the difference in redox behavior observed under N$_2$ atmosphere, there was no significant difference in electrocatalytic activity when comparing the unmethylated and methylated rhenium tpy complexes under CO$_2$ atmosphere. Previous research has shown that the methylated complex is less electron rich, as expected from the positively charged methylpyridinium group, compared to Re(κ^2-tpy)(CO)$_3$Cl. This resulted in lower reduction potentials and an additional reduction of the methylpyridinium moiety itself.

Under nitrogen, the unmethylated Re(κ^2-tpy)(CO)$_3$Cl compound shows a reversible first reduction event while the first reduction of the methylated analogue is predominantly irreversible. It is worth noting that the first reduction of Re(κ^2-tpy)(CO)$_3$Cl becomes irreversible in the presence

of CO_2. The irreversibility shows that CO_2 is reacting with the reduced complex (Figure 6). Additional reductions of both complexes are irreversible, even under N_2, which is a consequence of chloride dissociation. Under CO_2 atmosphere, a modest increase in current is observed signifying electrocatalytic CO_2 reduction. Plots of the peak current versus the square root of the scan rate from scan rate dependent cyclic voltammograms show linear behavior, which is consistent with diffusion controlled redox processes and homogeneous electroactive species.

INTRODUCTION

Guanine is a nucleobase found in both DNA and RNA. If this nucleobase is oxidized and damaged, then mutations can occur that have been linked to Alzheimer's, melanoma, prostate cancer, and diabetes.[8] It is redox active and has the lowest standard reduction potential amongst the nucleobases. Guanine have enhanced reactivity based on the solution conditions of its environment.[8,20]

Common amino acids have been previously studied such as tyrosine, cysteine, and tryptophan.[10,20] Cysteine is the most acidic of the three common redox active amino acids with a pK_a of 8.2 associated with its thiol. Cysteine is important in electron transfer carriers and mediators in photosystem II, class I ribonucleotide reductase, and DNA photolyse.[10,11] Cysteine residues can create an adduct with carboxylate bases like aspartate. Oxidation of cysteine goes through concerted EPT when using proton acceptor bases like acetate and phosphate. CysSH$^+$/CysSH is greater than 1.5 V vs NHE.[8,10]

Tyrosine has been studied more extensively. Tyrosine has a pK_a = 10.1 associated with the proton on the hydroxyl group. Tyrosine oxidation can be done by the addition of a M(bpy)$_3^{2+}$ to invoke EPT; however, when bases are added to the metal catalyst and tyrosine, then the pathway is MS-EPT. Like cysteine, tyrosine uses proton-coupled electron transfer (PCET) to avoid the build-up of charge.[9,10] PCET is a process in which proton and electron transfer events are coupled. The ability for concerted EPT allows for the avoidance of high energy protonated intermediates that could otherwise form.[9,11] Tyrosine is important as an electron transfer carrier in photosystem II. Proteins can interact with the tyrosine residue through an associated histidine base for oxidation.

The base acts as an EPT proton acceptor for the tyrosine to avoid intermediates like Tyr-OH$^{\cdot*}$. The primary equation being TyrOH-His base adduct to TyrO^{0}-*H-His via MS-EPT.[10]

Concerted electron-proton transfer (concerted EPT) is essentially the ability to transfer electrons or protons from orbitals of one donor to the orbitals of one acceptor.[4] The initial step of concerted EPT are always H-atom transfer (HAT) and electron-proton transfer (EPT). In HAT, one of the reactants transfers an electron and proton from the same bond. The main purpose of concerted EPT is the ability to avoid high-energy intermediates due to simultaneous transfer of the electron and proton. In EPT, the donor and acceptor orbitals are enabled to instantaneously transfer an electron and proton from donor to acceptor.[20]

Multisite electron-proton transfer (MS-EPT) is concerted EPT for multiple donors or acceptors. Different donors transferring electron and proton to one acceptor or vice versa. The kinetics of MS-EPT are affected by buffer base rather than by pH. It has been proven in one study about tyrosine that when proton-acceptor bases are added it accelerates the oxidation of the phenol. In the experiment focused on tyrosine, an adduct is initially formed by H-bond formation. The adduct then becomes associated with Os(bpy)$_3$$^{3+}$, the redox mediator in this case, and is followed by concerted EPT. An electron transfer occurs to the redox mediator, and proton transfer received by buffer base. The redox mediator and buffer base are spatially separated from one another. This spatial divide between the electron-proton acceptors and donors as well as the number of electrons and protons that are transferred are characteristic of MS-EPT.

One of the most common examples of PCET in biological system is found in photosystem II. Photosystem II is a homodimer that weights 650 kDa and can be found in the membrane of oxygenic photosynthetic organisms (most commonly green plants). Photosystem II is one of four key functional elements embedded in the hydrophobic thylakoid membrane of chloroplasts. The

PCET experienced in photosystem II involves oxygen-evolving complex (OEC) to catalyze photooxidation of water to oxygen. OEC is a Mn_4CaO_4 cluster that contains a chloride ion and the cluster interacts with all the protein subunits.[20,22] The Mn_4CaO_4 cluster has two pertinent roles: calcium plays critical role in oxygen-oxygen bond formation, and the Cl ion is a necessary cofactor.[21,20] The Kok cycle allows for four photons to accumulate four oxidizing equivalents in the OEC which releases oxygen.[20] The oxygen production is coupled with the transport of four protons across the thylakoid membrane from the stroma to the lumen.[21-23] This is commonly referred to as a proton gradient. The production of oxygen is coupled to the reduction of the plastoquione (PQ) to plastoquinol (PQH_2) via the net reaction.[21-23] This reduction is demanding on energy (0.884 V), because it requires four photons for one molecule of oxygen. [20]

Again, GMP oxidation has been linked to mutations associated with numerous diseases. GMP oxidation can occur through two difference pathways, concerted EPT or MS-EPT. One pathway will dominate when environmental conditions change. Understanding the mechanistic behavior of GMP oxidation lends to a better fundamental understanding at the nucleic acid level.

EXPERIMENTAL DETAILS

Sodium phosphate buffer (1:1 $H_2PO_4^{-}$/ HPO_4^{2-}; pKa 7.2) and acetic acid/sodium acetate buffer (pKa 4.7) were made with Milli-Q water for stock solutions. The cyclic voltammetry (CV) was performed with a three-electrode cell. The working electrode was tin-doped indium oxide (ITO) coated glass electrode. The reference electrode was microelectrode Ag/AgCl. The counter electrode was a platinum wire. Prior to experimentation, the ITO slides were extensively washed with MilliQ water (15 minutes), isopropanol (15 minutes), rinsed with Milli-Q water for 15 minutes, and allowed to air dry for 24 hours. When conducting the CVs, the potential read in the

positive directions from 0-1.3 V vs NHE at a scan rate of 100 mV/s. The CVs were taken in a series of buffer, buffer with metal complex, and then buffer, metal complex, and GMP. After every series, a new ITO plate would be used.

RESULTS

Cyclic voltammetry was again used to study the oxidation of GMP under different solution conditions. Due to sluggish electron transfer kinetics at the ITO electrode, $Ru(bpy)_3Cl_2$ was used as a redox mediator to facilitate the oxidation while the proton could be transferred under the right conditions to the solvent or the base component of the buffer. Cyclic voltammograms are shown below with the conditions specified in each caption.
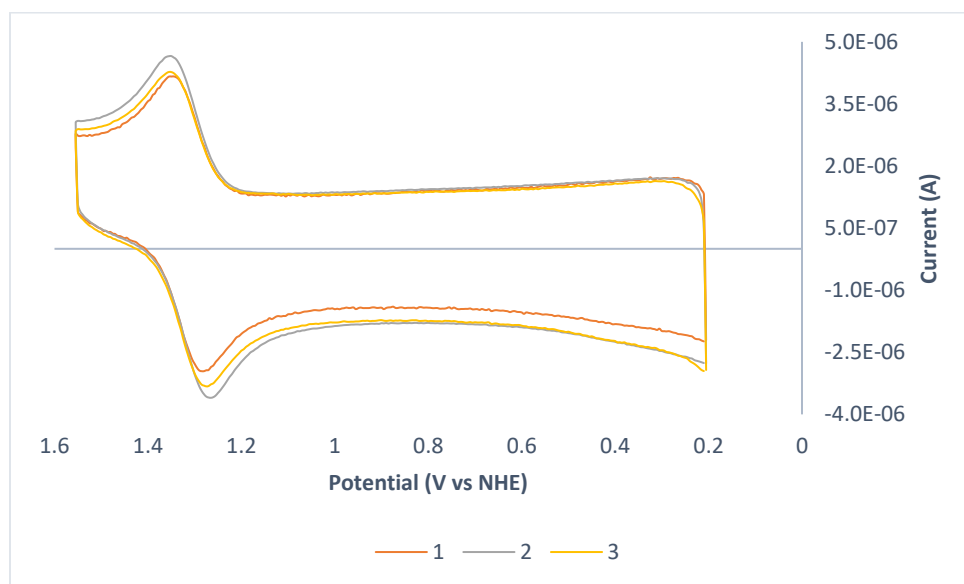
Figure 24. 0.05 M Sodium Acetate buffer with 20 μM of $Ru(bpy)_3Cl_2$. Each number representing a trial run.
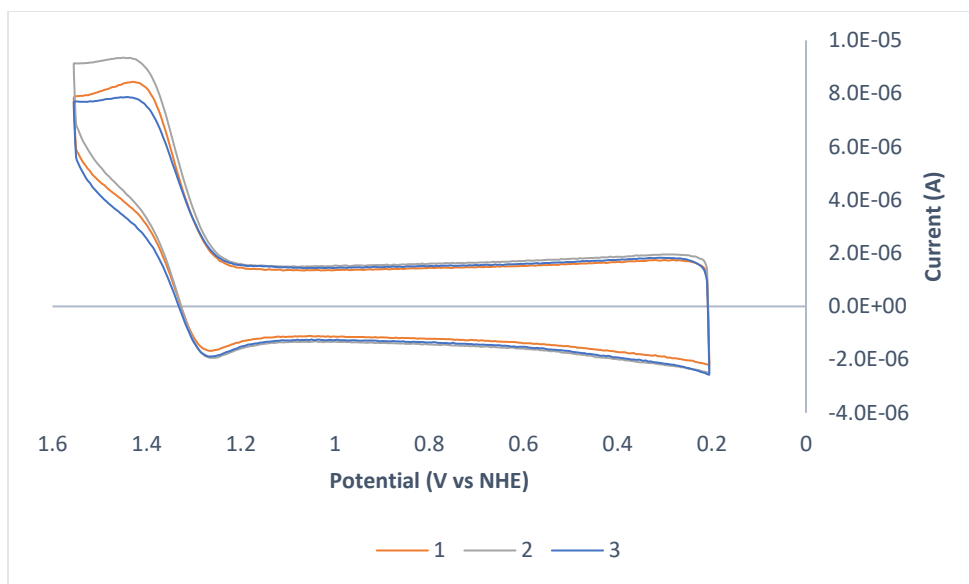
Figure 25. 0.05 M Sodium Acetate buffer with 20 µM of Ru(bpy)$_3$Cl$_2$ and 100 µM GMP. Each number representing a trial run.
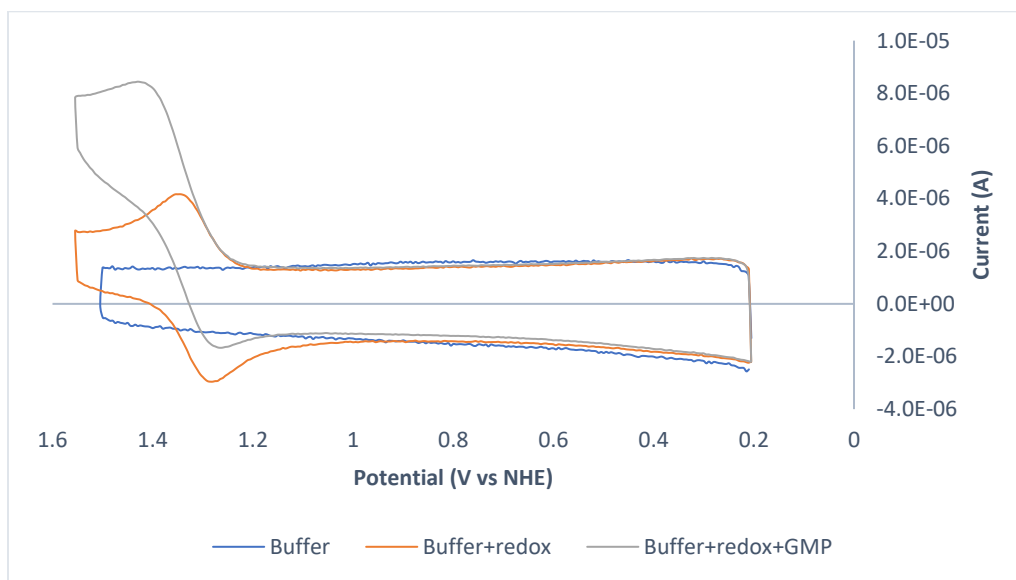
Figure 26. First trial of 0.05 M Sodium Acetate buffer with 20 µM of Ru(bpy)$_3$Cl$_2$ and 100 µM GMP. Each number representing a trial run.
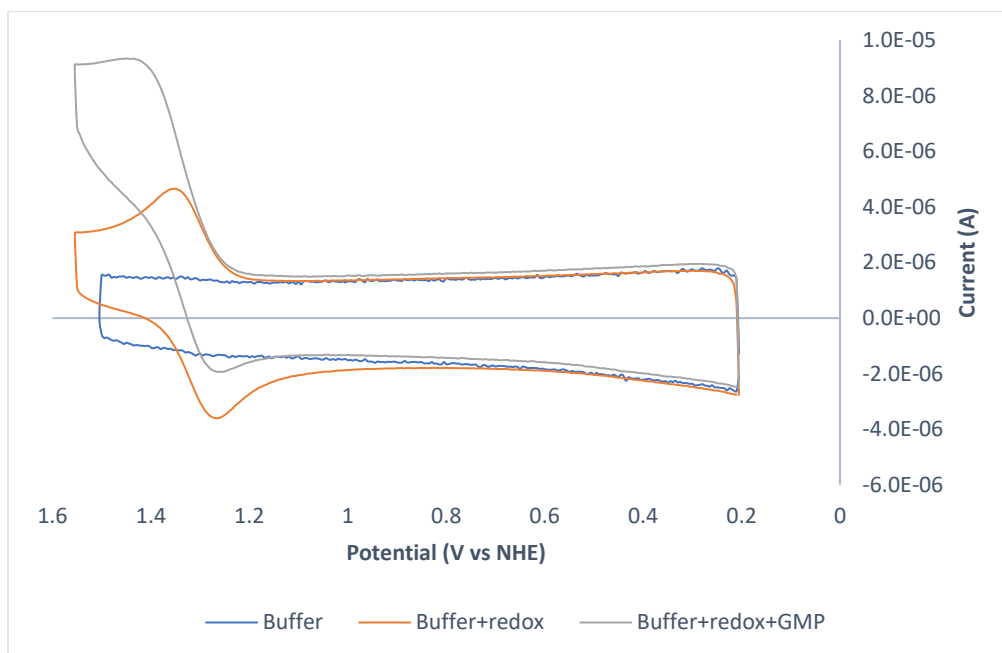
Figure 27. Second trial of 0.05 M Sodium Acetate buffer with 20 µM of Ru(bpy)$_3$Cl$_2$ and 100 µM GMP. Each number representing a trial run.
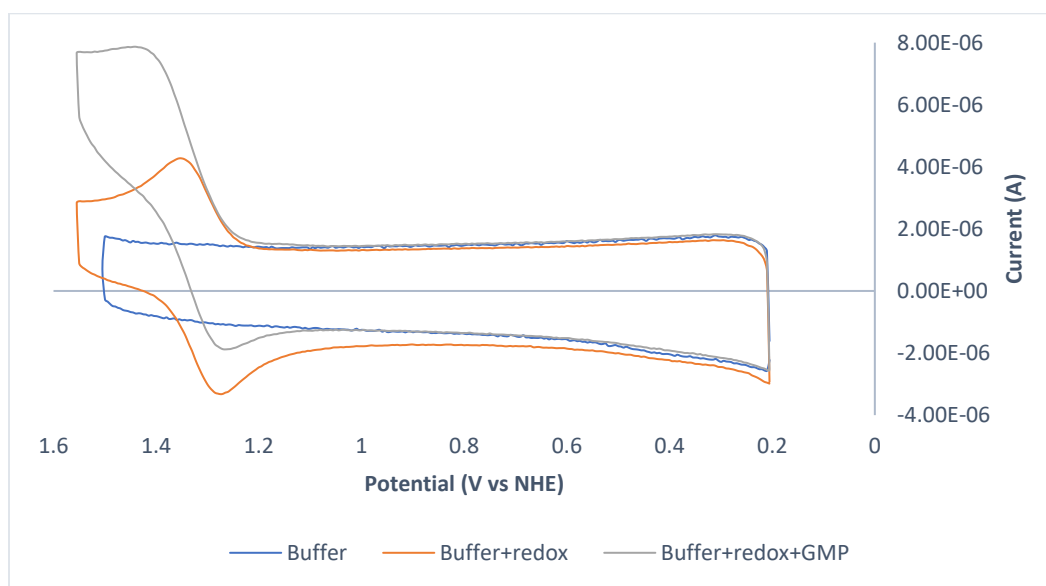
Figure 28. Third trial of 0.05 M Sodium Acetate buffer with 20 µM of Ru(bpy)$_3$Cl$_2$ and 100 µM GMP. Each number representing a trial run.
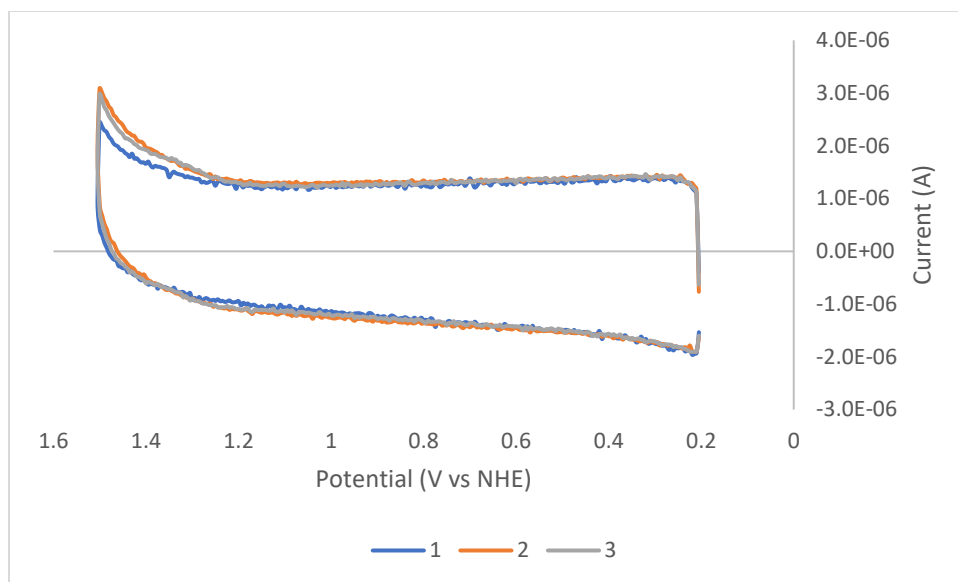
Figure 29. Na$_2$HPO4/NaH$_2$PO$_4$ buffer (0.05 M, 0.0083 M) only. Each number representing a trial run.
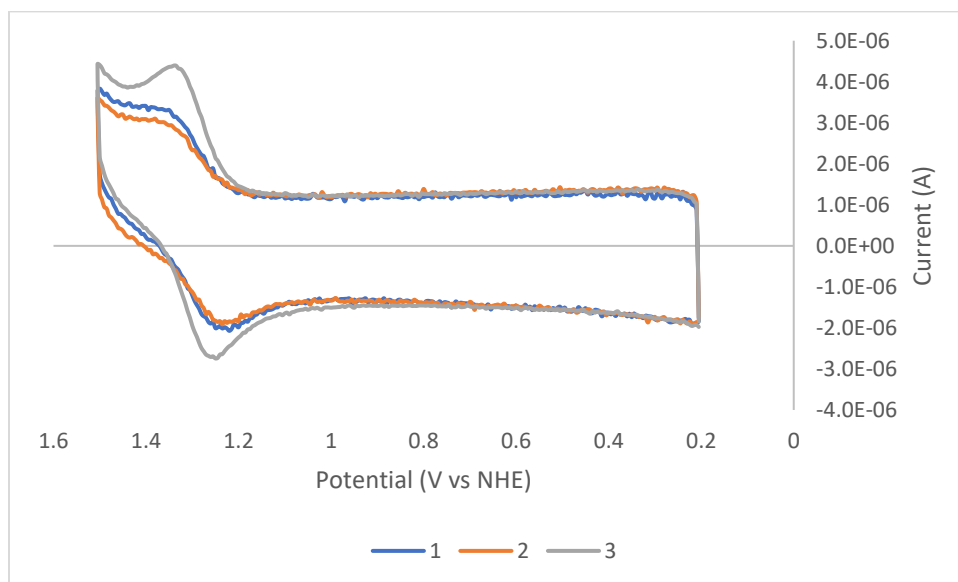
Figure 30. Na$_2$HPO$_4$/NaH$_2$PO$_4$ buffer (0.05 M, 0.0083 M) with 20 µM of Ru(bpy)$_3$Cl$_2$. Each number representing a trial run.
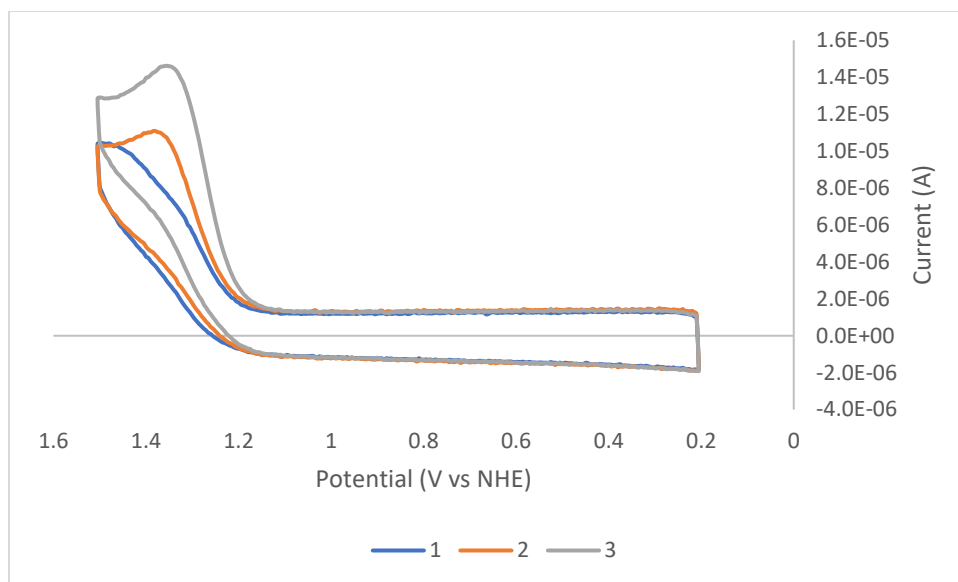
Figure 31. Na$_2$HPO$_4$/NaH$_2$PO$_4$ buffer (0.05 M, 0.0083 M) with 20 µM of Ru(bpy)$_3$Cl$_2$ and 100 µM GMP. Each number representing a trial run.
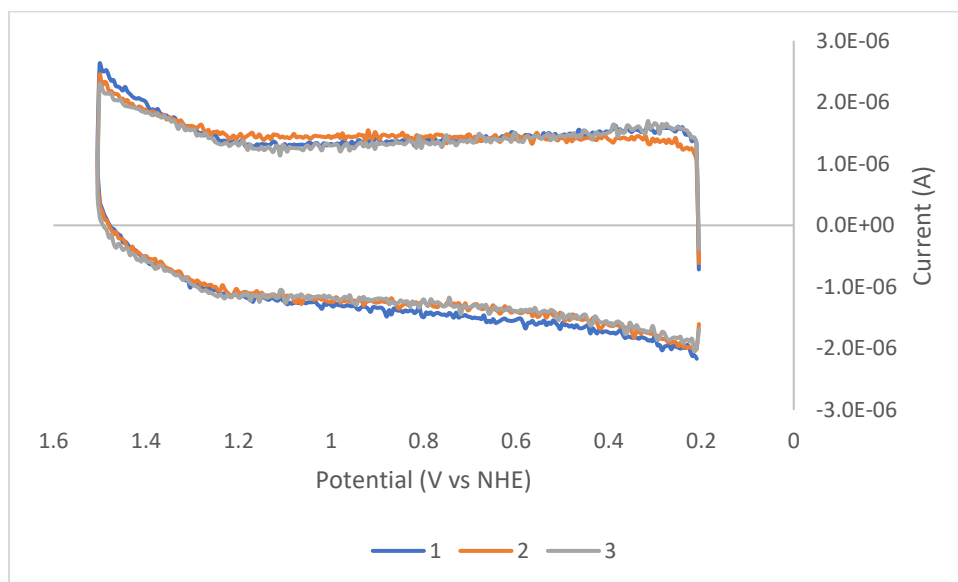
Figure 32. Na$_2$HPO$_4$/NaH$_2$PO$_4$ buffer (0.05 M, 0.03 M) only. Each number representing a trial run.
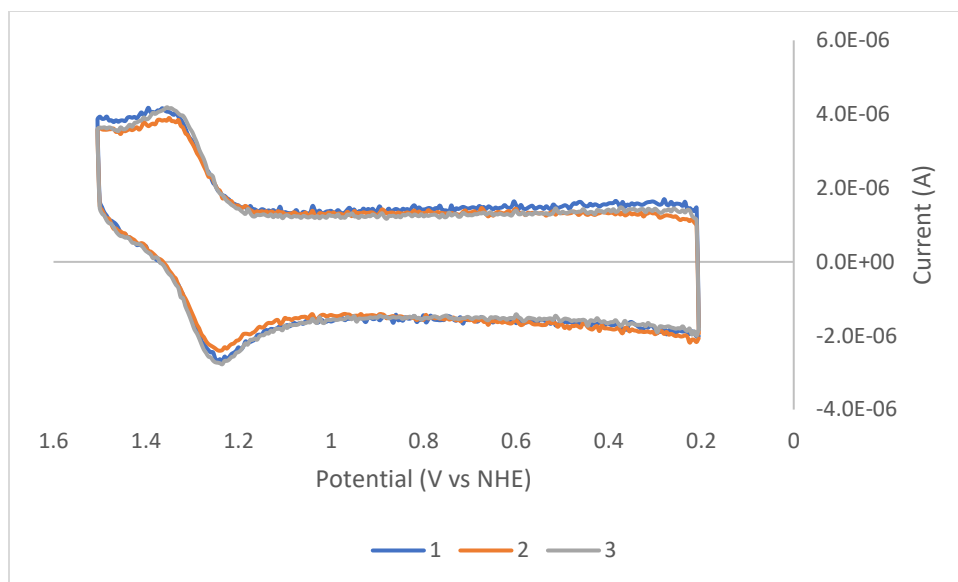
Figure 33. Na$_2$HPO$_4$/NaH$_2$PO$_4$ buffer (0.05 M, 0.03 M) with 20 µM of Ru(bpy)$_3$Cl$_2$. Each number representing a trial run.
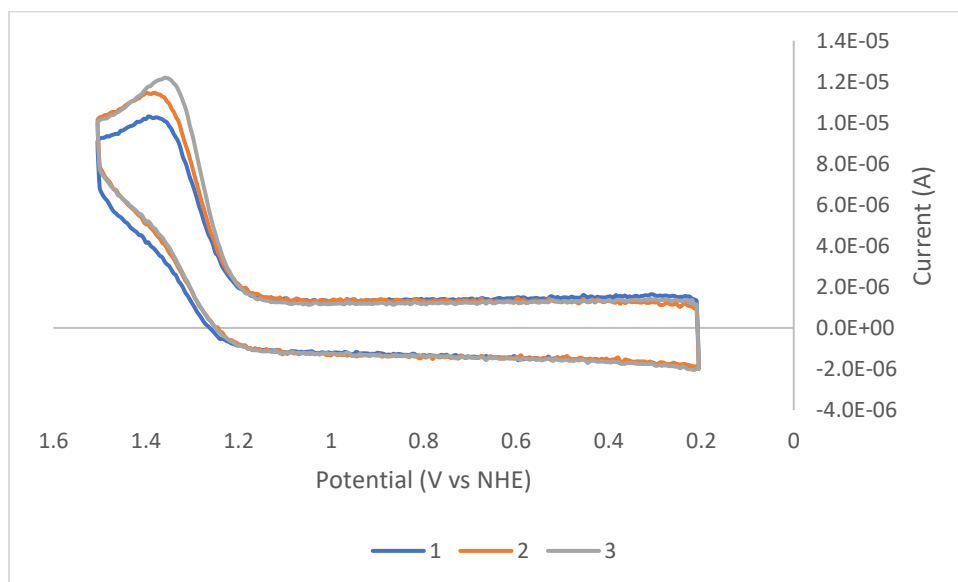
Figure 34. Na$_2$HPO$_4$/NaH$_2$PO$_4$ buffer (0.05 M, 0.03 M) with 20 µM of Ru(bpy)$_3$Cl$_2$ and 100 µM GMP. Each number representing a trial run.
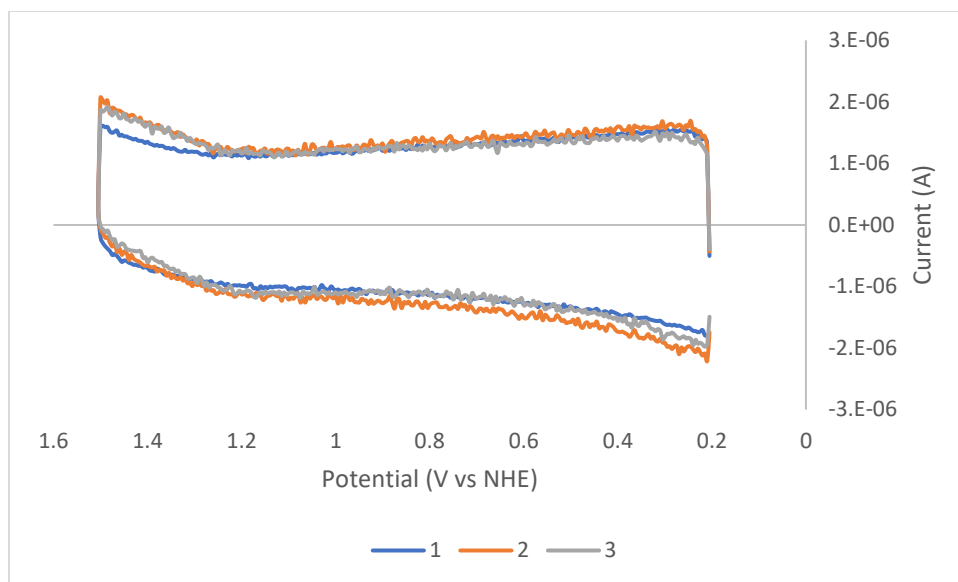
Figure 35. Na$_2$HPO$_4$/NaH$_2$PO$_4$ buffer (0.05 M, 0.07 M) only. Each number representing a trial run.
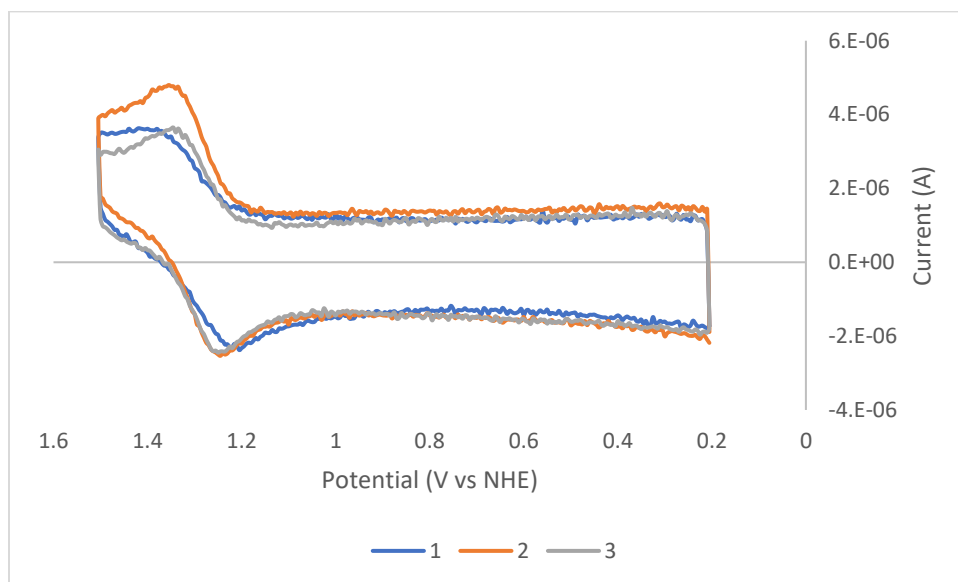
Figure 36. Na$_2$HPO$_4$/NaH$_2$PO$_4$ buffer (0.05 M, 0.07 M) with 20 µM of Ru(bpy)$_3$Cl$_2$. Each number representing a trial run.
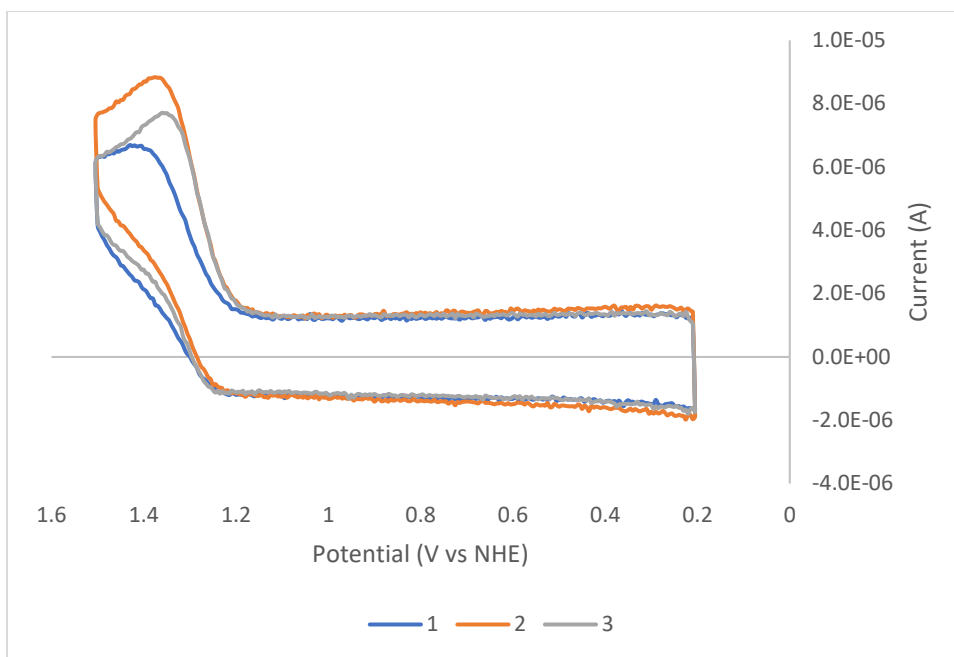
Figure 37. Na$_2$HPO$_4$/NaH$_2$PO$_4$ buffer (0.05 M, 0.07 M) with 20 μM of Ru(bpy)$_3$Cl$_2$ and 100 μM GMP. Each number representing a trial run.
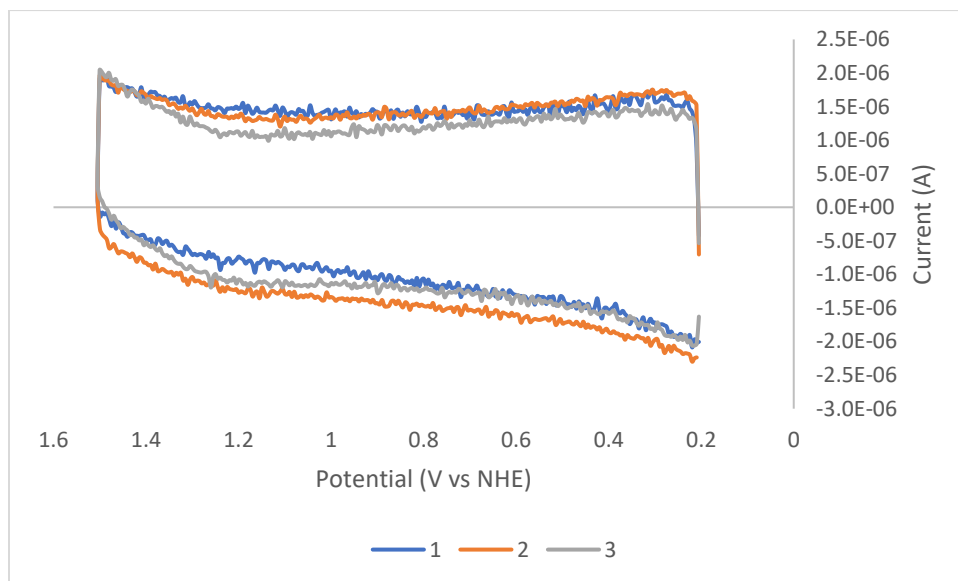
Figure 38. Na$_2$HPO$_4$/NaH$_2$PO$_4$ buffer (0.05 M, 0.13 M) only. Each number representing a trial run.
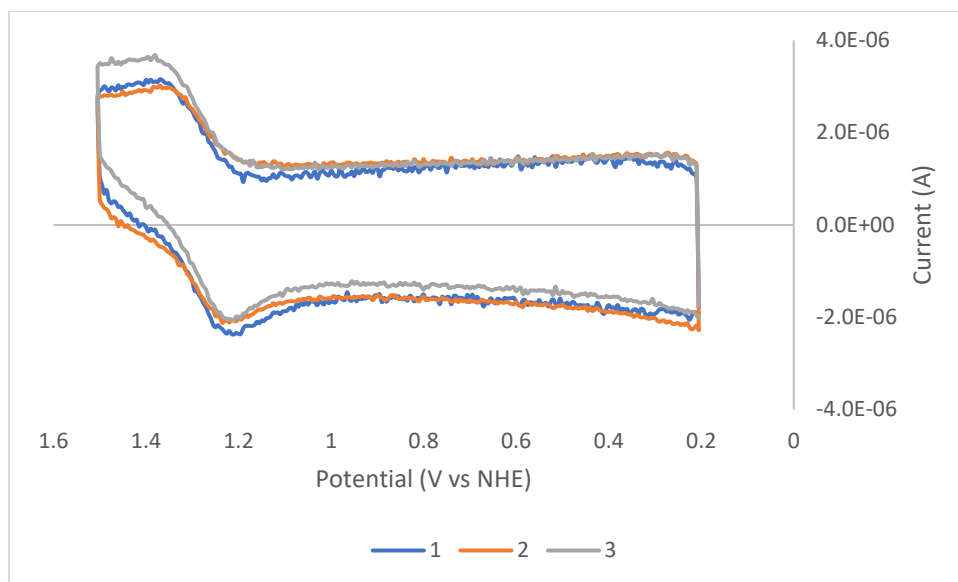
Figure 39. Na$_2$HPO$_4$/NaH$_2$PO$_4$ buffer (0.05 M, 0.13 M) with 20 µM of Ru(bpy)$_3$Cl$_2$. Each number representing a trial run.
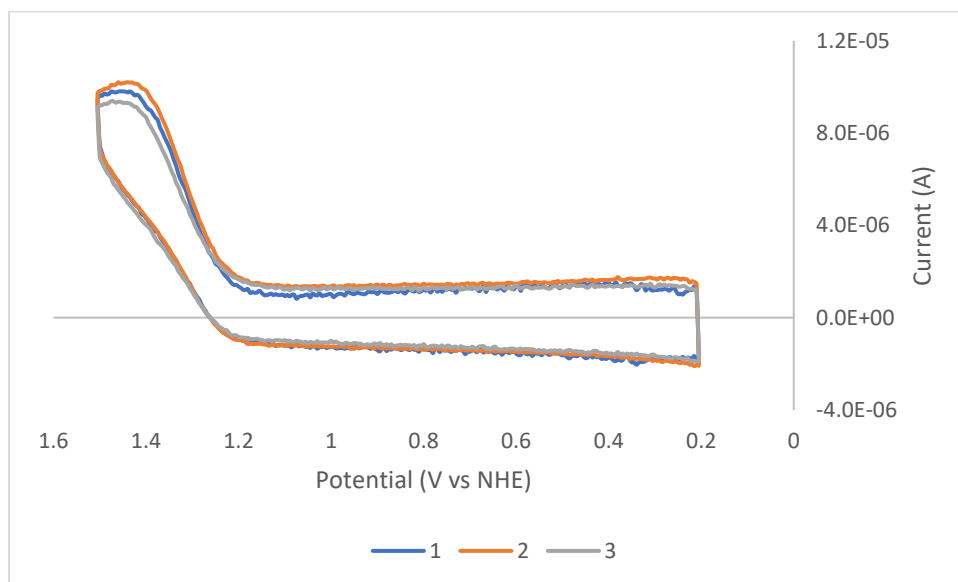
Figure 40. Na$_2$HPO$_4$/NaH$_2$PO$_4$ buffer (0.05 M, 0.13 M) with 20 µM of Ru(bpy)$_3$Cl$_2$ and 100 µM GMP. Each number representing a trial run.
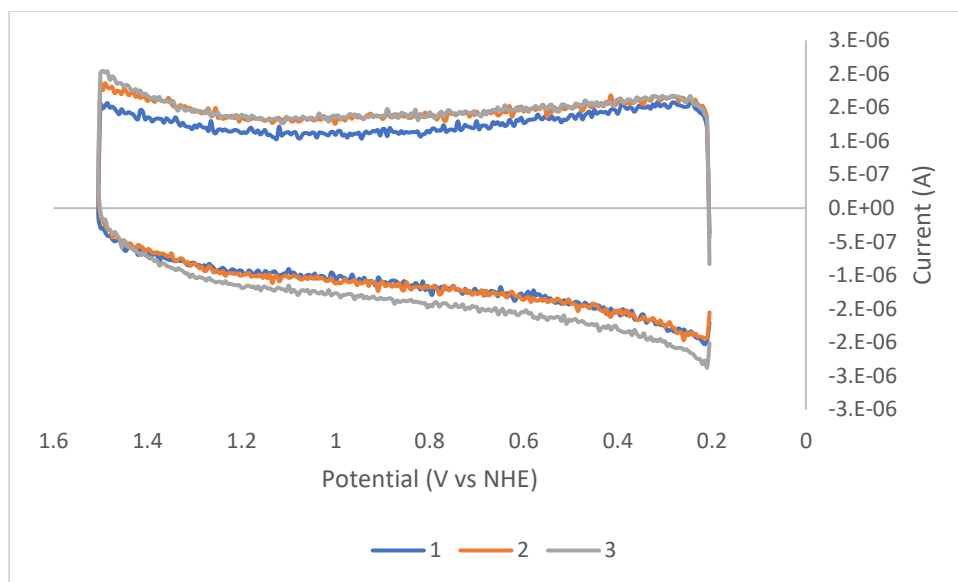
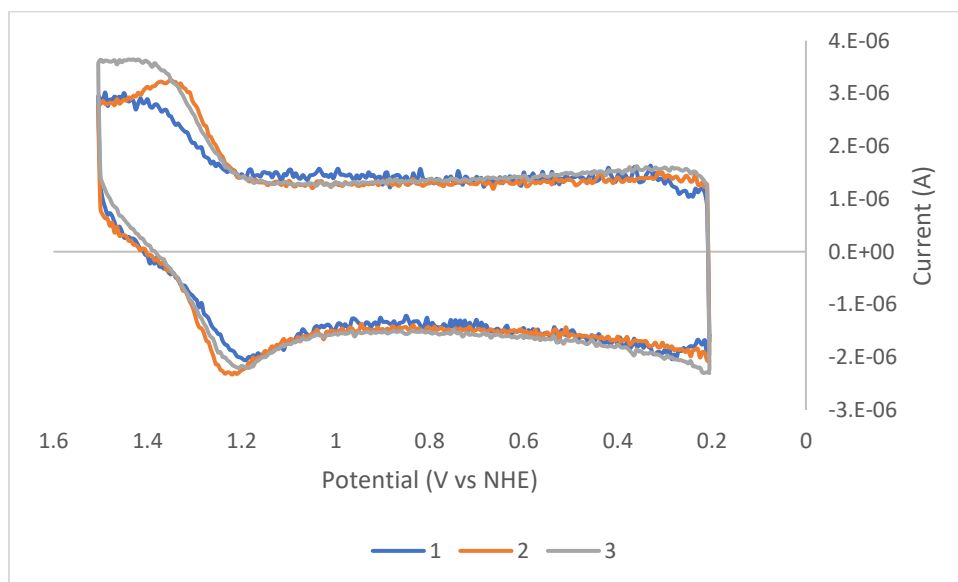**Figure 41.** Na$_2$HPO$_4$/NaH$_2$PO$_4$ buffer (0.05 M, 0.17 M) only. Each number representing a trial run.

Figure 42. Na$_2$HPO$_4$/NaH$_2$PO$_4$ buffer (0.05 M, 0.17 M) with 20 µM of Ru(bpy)$_3$Cl$_2$. Each number representing a trial run.
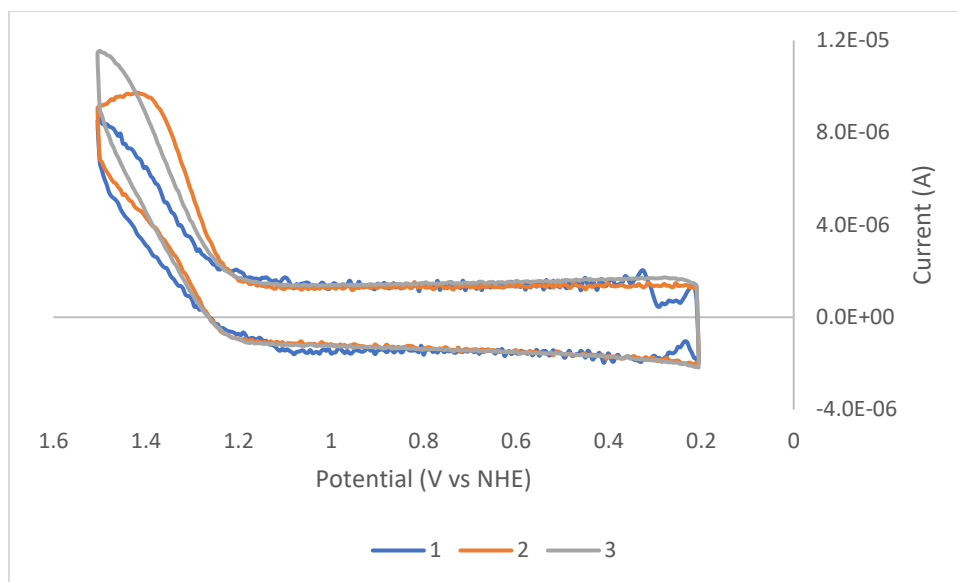
Figure 43. Na$_2$HPO$_4$/NaH$_2$PO$_4$ buffer (0.05 M, 0.17 M) with 20 µM of Ru(bpy)$_3$Cl$_2$ and 100 µM GMP. Each number representing a trial run.
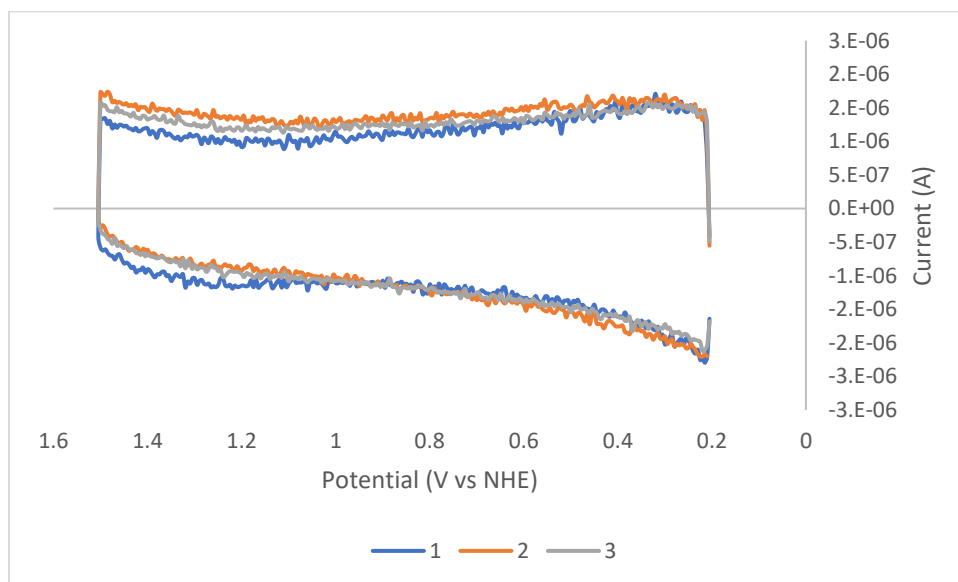
Figure 44. Na$_2$HPO$_4$/NaH$_2$PO$_4$ buffer (0.05 M, 0.22 M) only. Each number representing a trial run.
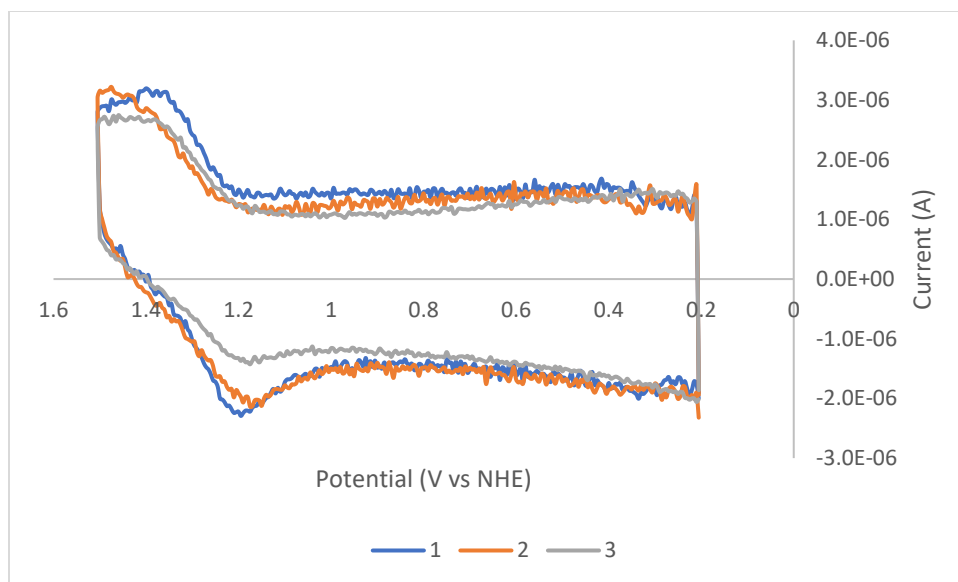
Figure 45. Na_2HPO_4/NaH_2PO_4 buffer (0.05 M, 0.22 M) with 20 µM of $Ru(bpy)_3Cl_2$. Each number representing a trial run.
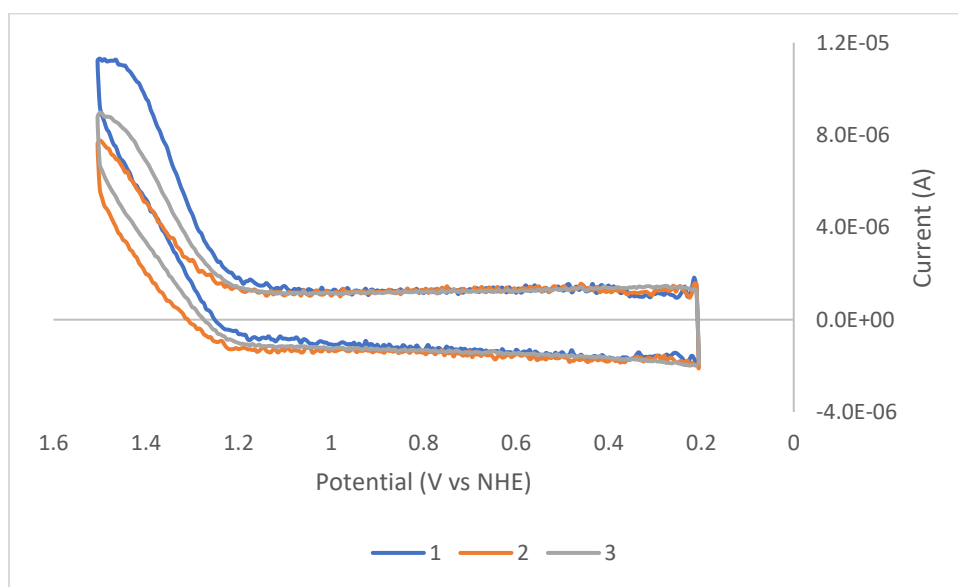
Figure 46. Na_2HPO_4/NaH_2PO_4 buffer (0.05 M, 0.22 M) with 20 µM of $Ru(bpy)_3Cl_2$ and 100 µM GMP. Each number representing a trial run.
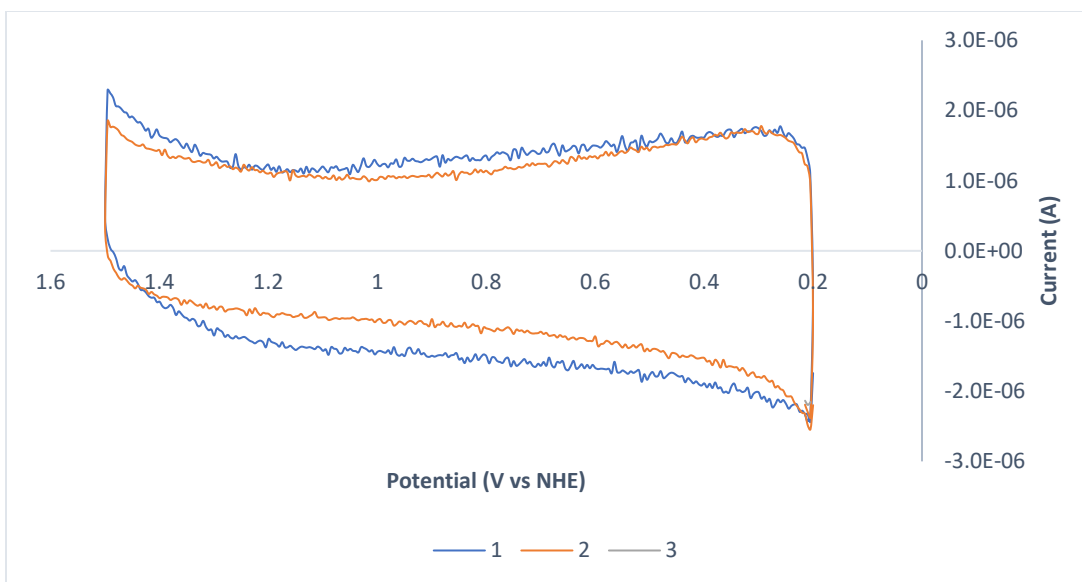
Figure 47. 1:1 Na$_2$HPO4/NaH$_2$PO$_4$ buffer (0.05 M) only. Each number representing a trial run.

Figure 48. 1:1 Na$_2$HPO4/NaH$_2$PO$_4$ buffer (0.05 M) with 5 µM of Ru(bpy)$_3$Cl$_2$. Each number representing a trial run.
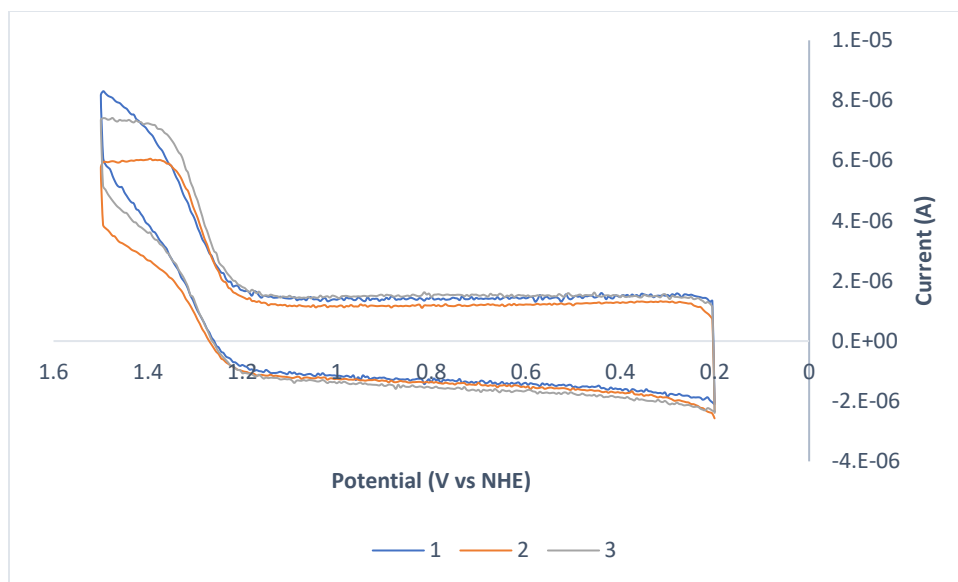
Figure 49. 1:1 Na$_2$HPO4/NaH$_2$PO$_4$ buffer (0.05 M) with 5 µM of Ru(bpy)$_3$Cl$_2$ and 100 µM GMP. Each number representing a trial run.
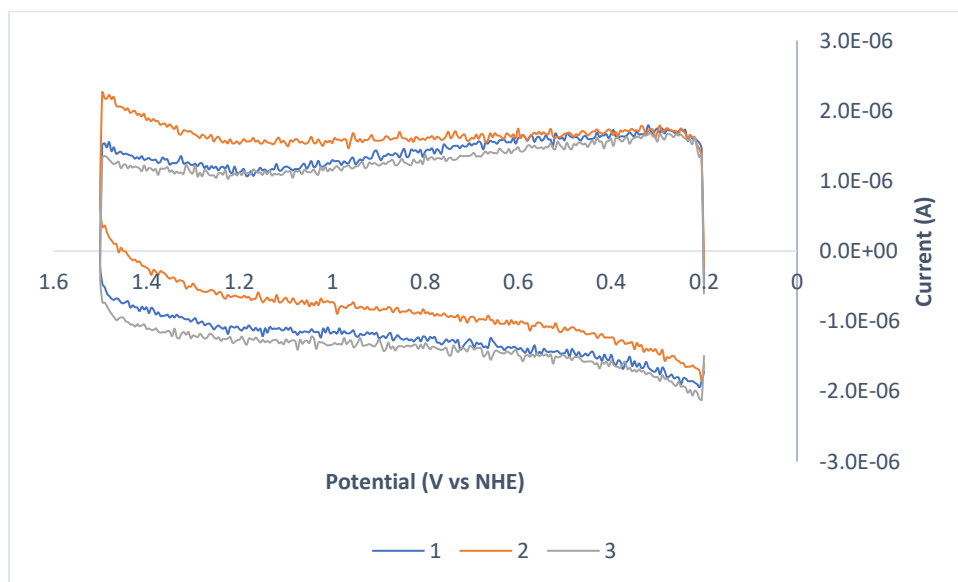
Figure 50. 1:1 Na$_2$HPO4/NaH$_2$PO$_4$ buffer (0.05 M) only. Each number representing a trial run.

Figure 51. 1:1 Na$_2$HPO4/NaH$_2$PO$_4$ buffer (0.05 M) with 10 µM of Ru(bpy)$_3$Cl$_2.$ Each number representing a trial run.
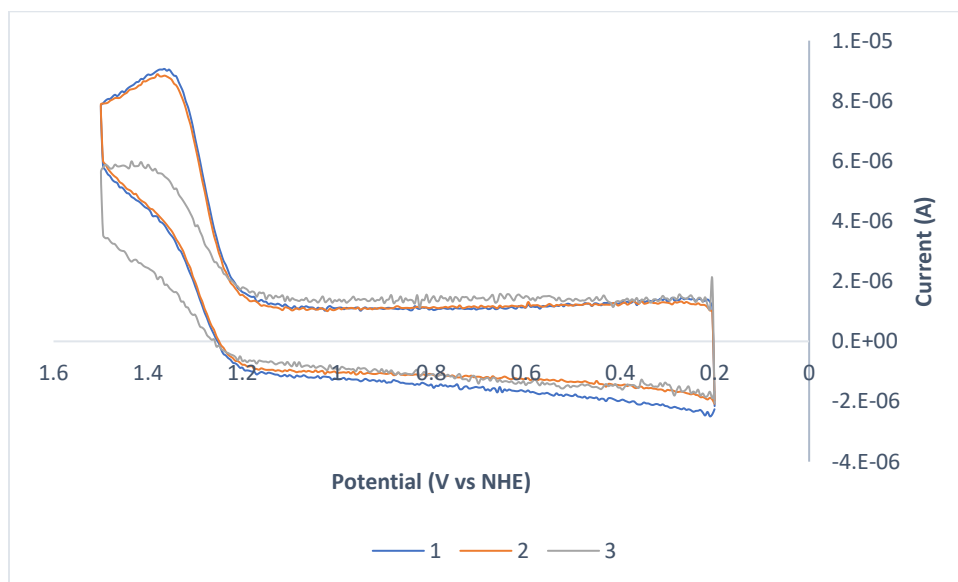
Figure 52. 1:1 Na$_2$HPO4/NaH$_2$PO$_4$ buffer (0.05 M) with 10 µM of Ru(bpy)$_3$Cl$_2$ and 100 µM GMP. Each number representing a trial run.
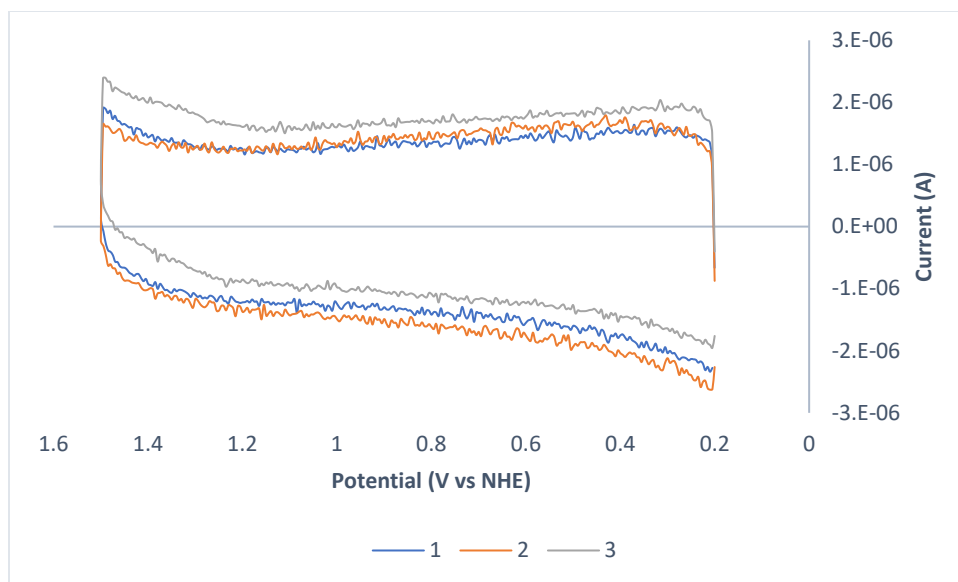
Figure 53. 1:1 Na$_2$HPO4/NaH$_2$PO$_4$ buffer (0.05 M) only. Each number representing a trial run.
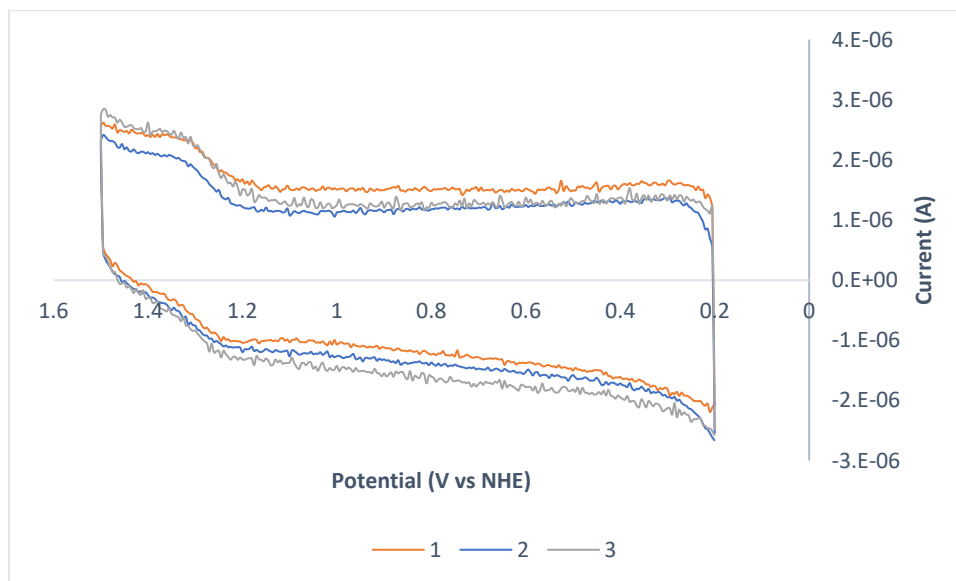

Figure 54. 1:1 Na$_2$HPO4/NaH$_2$PO$_4$ buffer (0.05 M) with 20 µM of Ru(bpy)$_3$Cl$_2$. Each number representing a trial run.
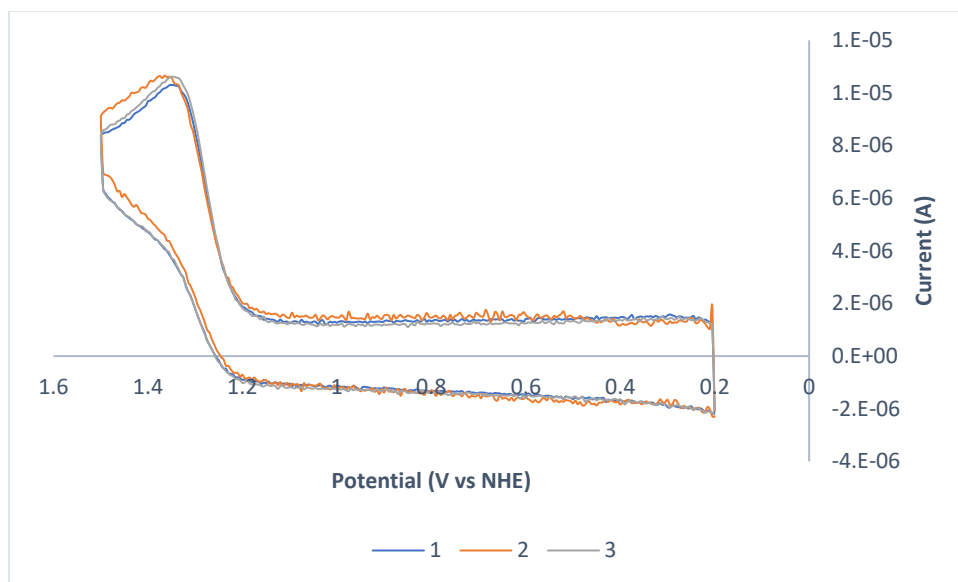
Figure 55. 1:1 Na$_2$HPO4/NaH$_2$PO$_4$ buffer (0.05 M) with 20 µM of Ru(bpy)$_3$Cl$_2$ and 100 µM GMP. Each number representing a trial run.
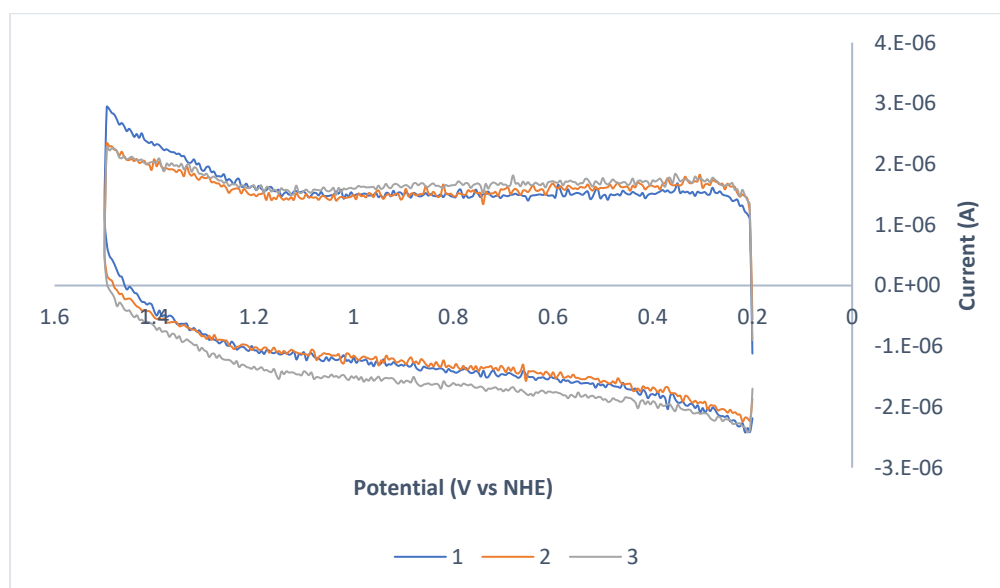
Figure 56. 1:1 Na$_2$HPO4/NaH$_2$PO$_4$ buffer (0.05 M) only. Each number representing a trial run.
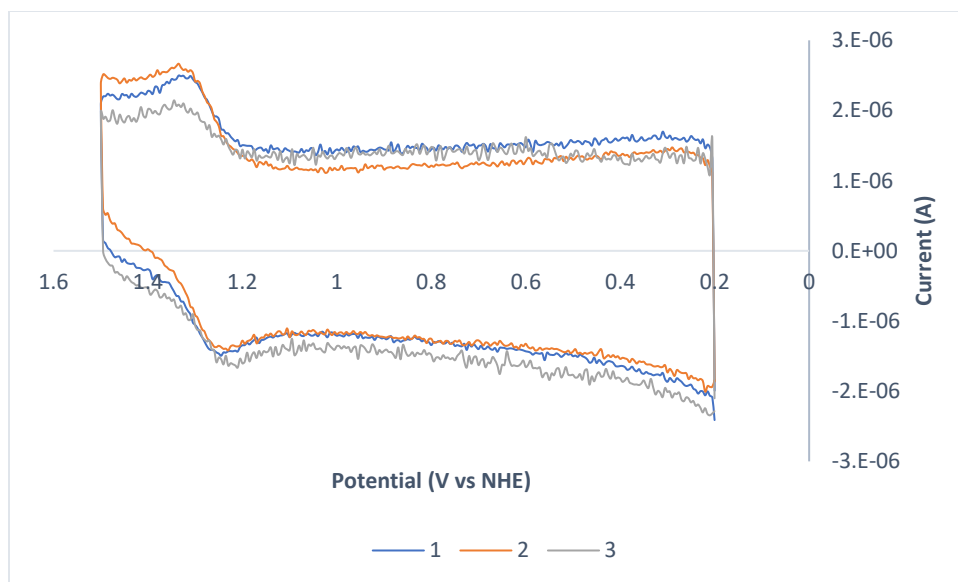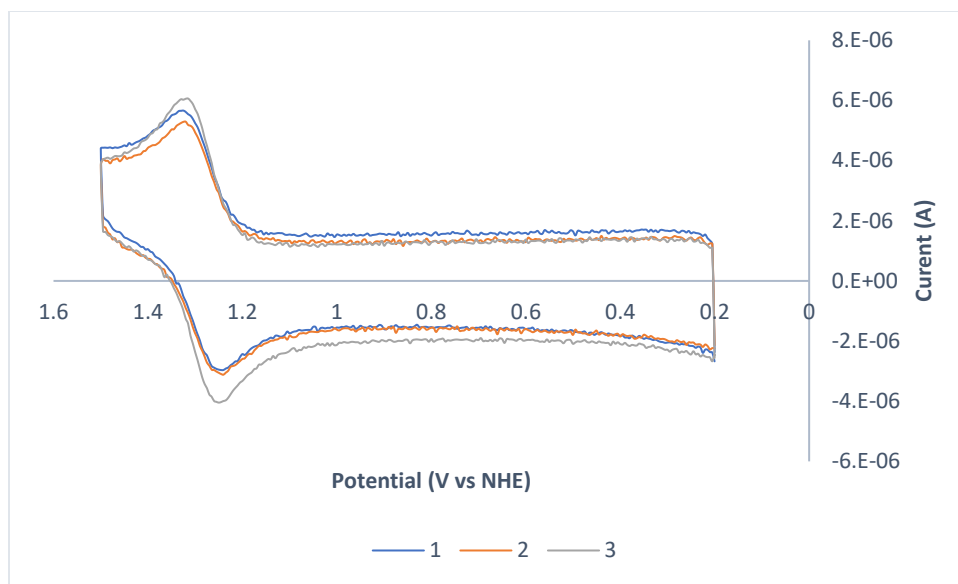
Figure 57. 1:1 Na$_2$HPO4/NaH$_2$PO$_4$ buffer (0.05 M) with 30 µM of Ru(bpy)$_3$Cl$_2$. Each number representing a trial run.
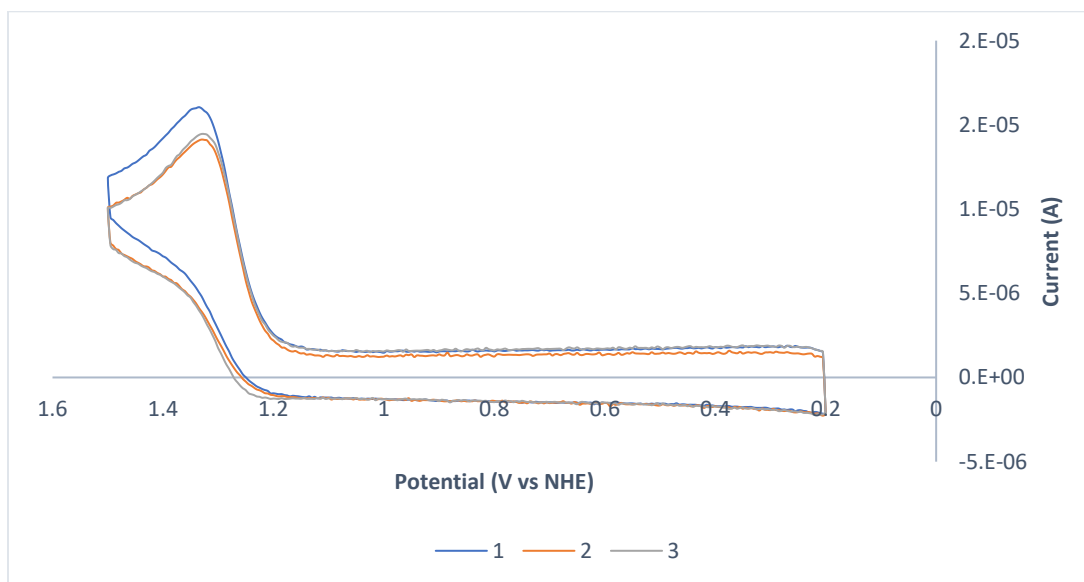
Figure 58. 1:1 Na$_2$HPO4/NaH$_2$PO$_4$ buffer (0.05 M) with 30 µM of Ru(bpy)$_3$Cl$_2$ and 100 µM GMP. Each number representing a trial run.
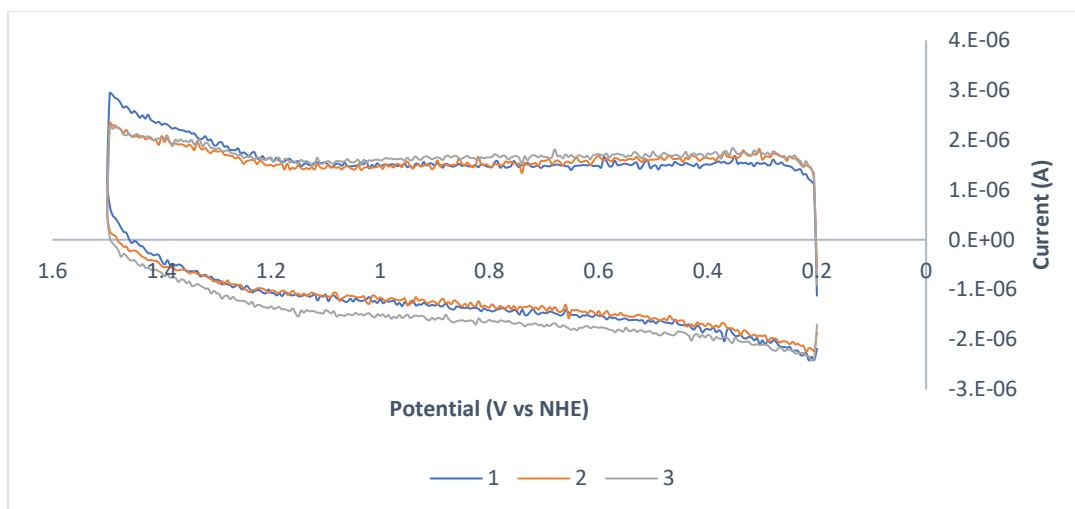
Figure 59. 1:1 Na$_2$HPO4/NaH$_2$PO$_4$ buffer (0.05 M) only. Each number representing a trial run.
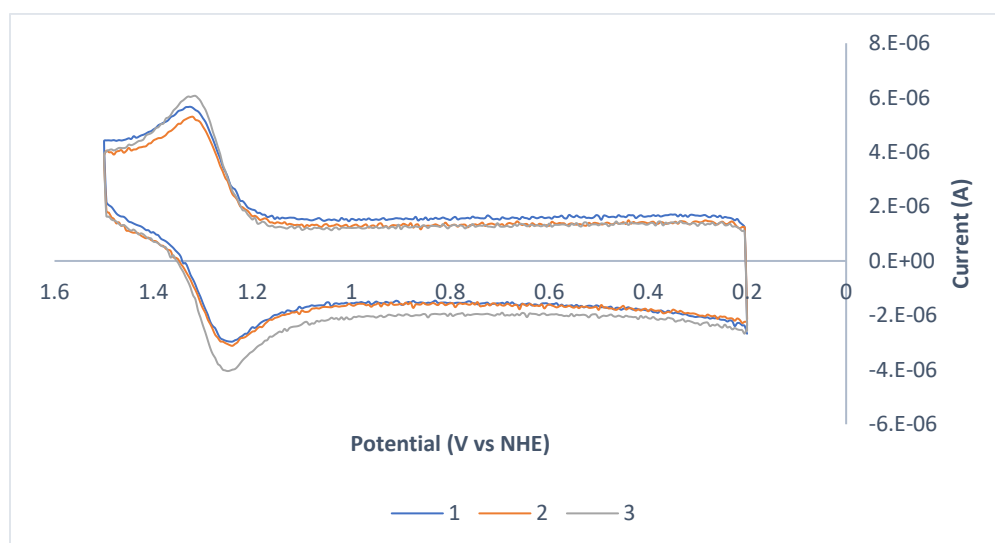
Figure 60. 1:1 Na$_2$HPO4/NaH$_2$PO$_4$ buffer (0.05 M) with 40 μM of Ru(bpy)$_3$Cl$_2$. Each number representing a trial run.
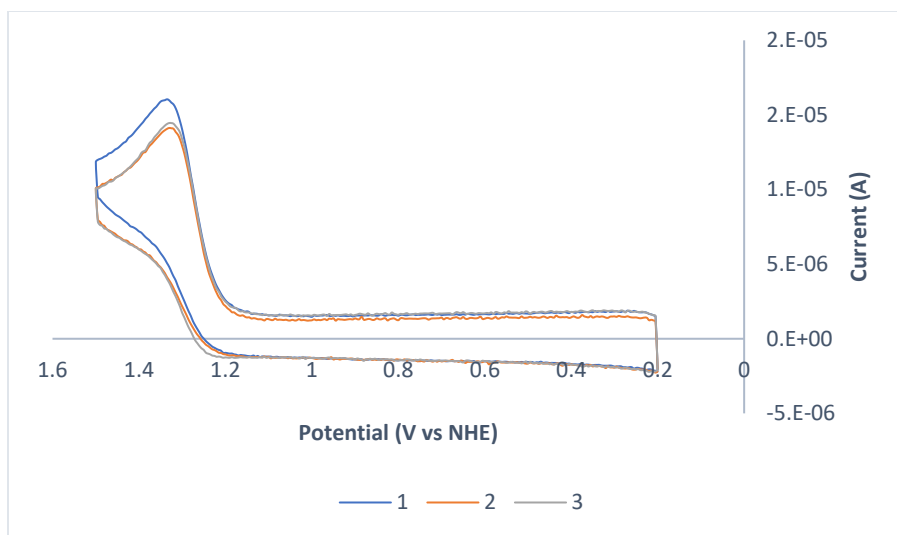
Figure 61. 1:1 Na$_2$HPO4/NaH$_2$PO$_4$ buffer (0.05 M) with 40 µM of Ru(bpy)$_3$Cl$_2$ and 100 µM GMP. Each number representing a trial run.
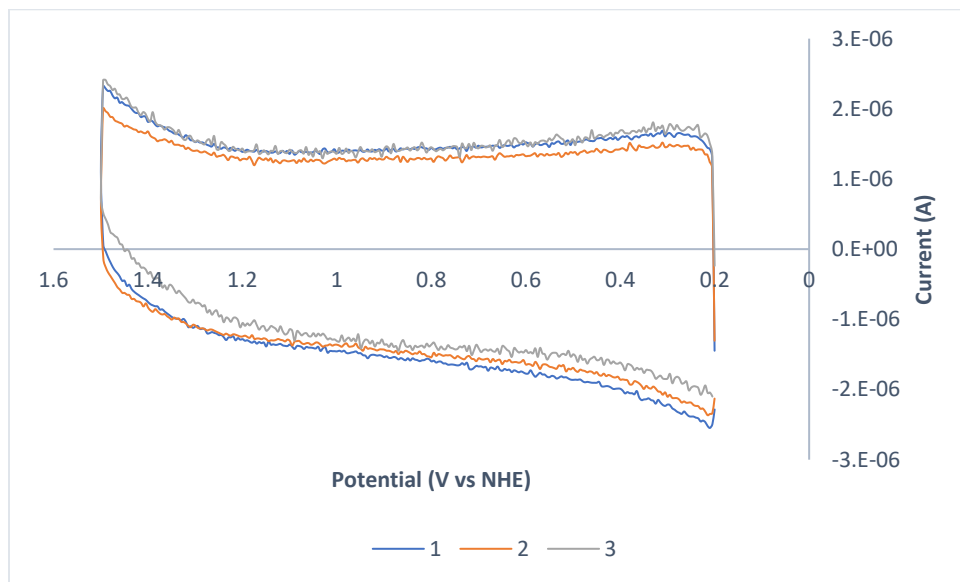
Figure 62. 1:1 Na$_2$HPO4/NaH$_2$PO$_4$ buffer (0.05 M) only. Each number representing a trial run.
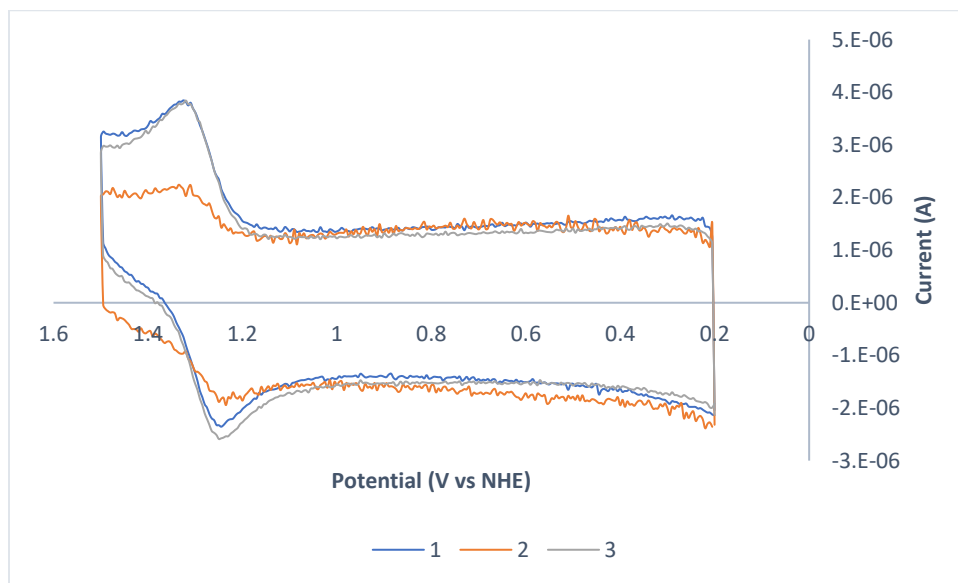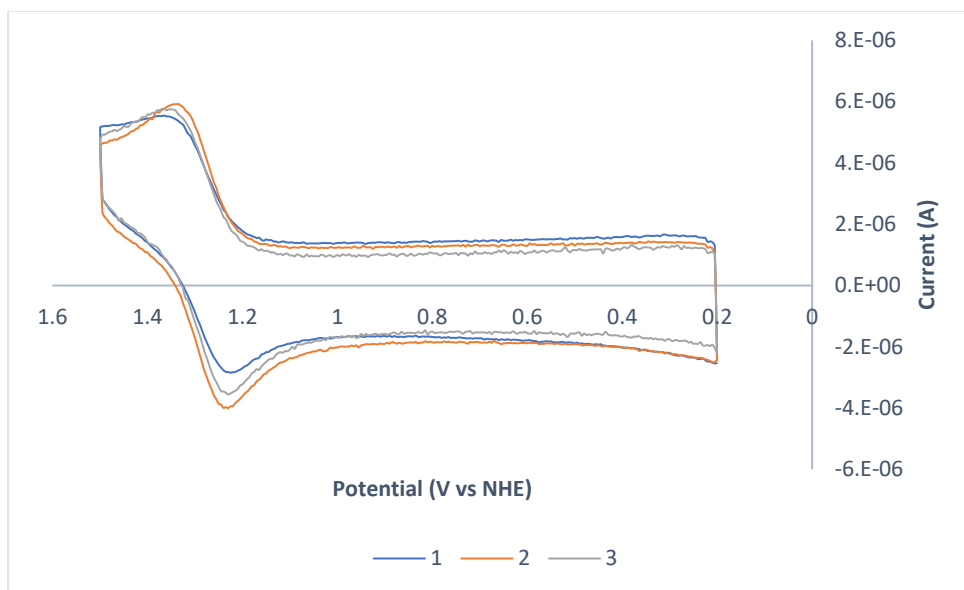
Figure 63. 1:1 Na$_2$HPO4/NaH$_2$PO$_4$ buffer (0.05 M) with 50 µM of Ru(bpy)$_3$Cl$_2$. Each number representing a trial run.
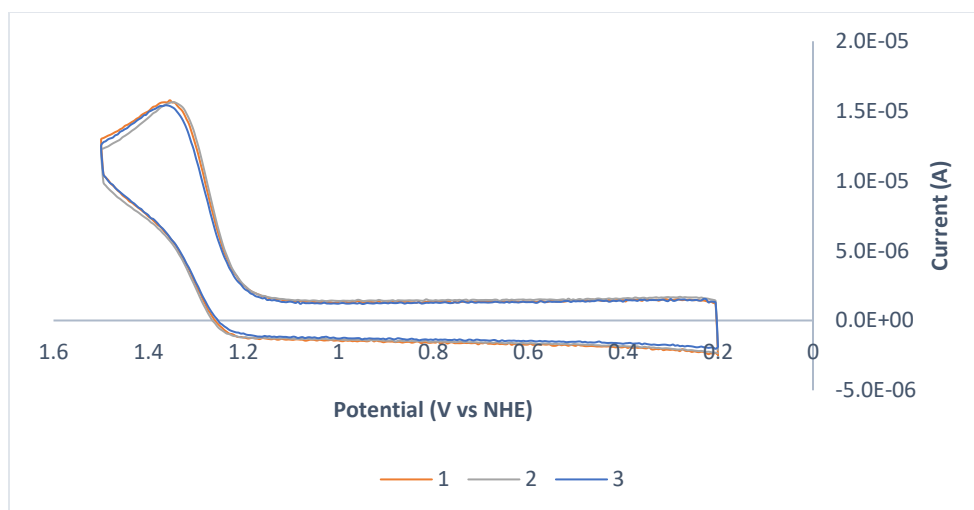
Figure 64. 1:1 Na$_2$HPO4/NaH$_2$PO$_4$ buffer (0.05 M) with 50 µM of Ru(bpy)$_3$Cl$_2$ and 100 µM GMP. Each number representing a trial run.

DISCUSSION

The cyclic voltammograms (CVs) employing the acetate buffer have well-defined peaks. The redox mediator and buffer CV have the expected redox event associated with the ruthenium complex, which corresponds to the Ru(III/II) couple. Although the resulting CVs feature a well-behaved redox process, the oxidation peak of GMP in the acetate solution is lower than that observed in phosphate buffer. The results indicate that acetate, at a more acidic pH (4.06) in comparison to the phosphate buffer (6.09), does not aid in the proton exchange. Thus, there is no enhanced reactivity seen when acetate buffer is used.

As the acidity of the phosphate solution was increased, the reduction and oxidation waves were less defined. The increase in acidity correlated to less current associated with the peaks for both the redox mediator CVs and those with GMP. The need for more basic buffer solutions correlates with the MS-EPT mechanism. Based on the varying concentrations of redox mediator, the oxidation of GMP occurs at 1.3 V vs NHE. No additional current increase is seen after 20 μM redox mediator; the current maxes out at 2 amperes. This current plateau is consistent with saturation conditions, in which the oxidation kinetics become independent of redox mediator concentration.

CONCLUSIONS

In Chapter 1, two rhenium catalysts for CO_2 reduction were studied side-by-side as part of a fundamental study to understand the effect on catalysis of adding a redox-active pendant to the bidentate metal-binding group. Under CO_2 as the atmosphere, a catalytic reaction between CO_2 and the reduced complexes was apparent by the increase in current relative to CVs obtained under N_2 atmosphere. From scan rate dependent CVs, the redox processes associated with these compounds were found to be diffusion controlled. Interesting reactivity at the first reduction was observed for the unmethylated rhenium tpy compound. However, the relatively low reactivity compared to known rhenium systems indicates that these catalysts are not promising candidates for improved systems for CO_2 reduction. The design of new ligands for enhanced reactivity will be the subject of future projects to develop better catalysts with lower overpotentials, high activity and selectivity, and with good stability for long-term catalytic CO_2 reduction.

GMP is an important component in understanding the basic redox reactivity of DNA and RNA, which may facilitate our understanding of how multiple disease states originate. In Chapter 2, it would found that increasing the acidity of solutions with GMP did not facilitate its oxidation. In contrast, more basic solutions, particularly those of phosphate buffer, assisted the oxidation of GMP, consistent with a MS-EPT mechanism. Basic environments allow more facile oxidation as the proton associated with removing an electron from GMP is effectively managed. PCET avoids high energy intermediates and the build-up of charge. The electrochemistry studies will be used in future studies to calculate the kinetic rates and provide the foundation for elucidating the oxidation pathways that GMP favors under specific conditions.

BIBLIOGRAPHY

1. Chabolla, Steven A., et al. "Combined Steric and Electronic Effects of Positional
   Substitution on Dimethyl-Bipyridine Rhenium(I)Tricarbonyl Electrocatalysts for the
   Reduction of CO 2." *Inorganica Chimica Acta*, vol. 422, 2014, pp. 109–113.,
   doi:10.1016/j.ica.2014.07.007.

2. http://www.eia.gov/totalenergy/data/monthly/pdf/sec1_3.pdf

3. http://www.eia.gov/todayinenergy/detail.cfm?id=26212

4. Sawyer, Donald T., et al. *Electrochemistry for Chemists*. Wiley-Interscience, 1995.

5. Civitello, Edgar R., et al. "Spectroscopic and Crystallographic Characterization of
   Tricarbonylchloro(Sigma.2-Terpyridyl)Rhenium. 2D-NMR Evidence for a Linkage
   Isomerization Reaction." *Inorganic Chemistry*, vol. 32, no. 2, 1993, pp. 237–241.,
   doi:10.1021/ic00054a022.

6. Baker, A David, and Robert J Morgan. "2,2':4,4':4',4''-Quaterpyridyl: A Building Block for
   the Preparation of Novel Redox Reagents. 1. Preparation and Quaternization." *Journal of
   Organic Chemistry*, vol. 55, 1990, pp. 1986–1993.

7. Wolf, Paul De, et al. "New 2,2′:4,4″:4′,4‴-Quaterpyridyl Transition Metal Complexes."
   Inorganica Chimica Acta, vol. 355, 2003, pp. 280–285., doi:10.1016/s0020-
   1693(03)00370-0.

8. Fleming, Aaron M., et al. "Rates of Chemical Cleavage of DNA and RNA Oligomers
   Containing Guanine Oxidation Products." *Chemical Research in Toxicology*, vol. 28, no.
   6, 2015, pp. 1292–1300., doi:10.1021/acs.chemrestox.5b00096.

9. Gagliardi, Christopher J., et al. "Concerted Electron–Proton Transfer (EPT) in the Oxidation
   of Tryptophan with Hydroxide as a Base." *Journal of the American Chemical Society*,
   vol. 133, no. 49, 2011, pp. 19594–19597., doi:10.1021/ja207379n.

10. Gagliardi, Christopher J., et al. "Concerted Electron–Proton Transfer (EPT) in the Oxidation of Cysteine." *The Journal of Physical Chemistry C*, vol. 119, no. 13, 2015, pp. 7028–7038., doi:10.1021/acs.jpcc.5b00368.

11. Goyal, Rajendra N., et al. "Electrochemical Oxidation of Guanosine-5′-Monophosphate at the Pyrolytic Graphite Electrode." *Journal of the Chemical Society, Perkin Transactions 2*, no. 5, 2001, pp. 832–837., doi:10.1039/b006076n.

12. Savéant, Jean-Michel. "Molecular Catalysis of Electrochemical Reactions. Mechanistic Aspects." *Chemical Reviews*, vol. 108, no. 7, 2008, pp. 2348–2378., doi:10.1021/cr068079z.

13. Lewis; Nocera; *Proc. Natl. Acad. Sci. USA* **2006**, *103*, 15729

14. Wigley TML, Richels R, Edmonds JA; *Nature* **1996,** 379, 240–243.

15. Maier-Reimer E, Hasselmann K; *Climate Dyn* **1987,** 2, 63–90.

16. Intergovernmental Panel on Climate Change; *Climate Change 2001, Synthesis Report Summary for Policymakers* (Intergovernmental Panel on Climate Change, Washington, DC), Third Assessment Report**. 2001**

17. W. Song, Z. Chen, M. K. Brennaman, J. J. Concepcion, A. T. Patrocinio, N. Y. Murakami Iha, T. J. Meyer; *Pure Appl. Chem***. 2011***, 83*, 749–768.

18. Love; *Chem. Commun*. **2012**, *48*, 1392.

19. E. E. Benson, C. P. Kubiak, A. J. Sathrum, J. M. Smieja; *Chem. Soc. Rev*. **2009**, *38*, 89.

20. Weinberg, David R., et al. "Proton-Coupled Electron Transfer." *Chemical Reviews*, vol. 112, no. 7, 2012, pp. 4016–4093., doi:10.1021/cr200177j.

21. Taiz, L.; Zeiger, E.; Plant Physiology; Fourth Edition; Sinauer Associates, Inc., 2006

22. https://www.britannica.com/science/photosynthesis/The-pathway-of-electrons

23. http://www.life.illinois.edu/govindjee/ZSchemeG.html

KAYLA MILANO

EDUCATION

B.A. Biochemistry, Austin Peay State University, December 2014

TEACHING EXPERIENCE

Head Teaching Assistant, 2018

University of Mississippi

Course: Organic Chemistry

Teaching Assistant, 2015-2018

University of Mississippi

Course: Organic Chemistry